University of Northern Iowa
UNI ScholarWorks

Dissertations and Theses @ UNI | Student Work

2018

Sand distribution effect on three dimensional printed sand properties

Kip Woods
University of Northern Iowa

Let us know how access to this document benefits you

Copyright ©2018 Kip Woods
Follow this and additional works at: https://scholarworks.uni.edu/etd

 Part of the Materials Science and Engineering Commons

Recommended Citation

Woods, Kip, "Sand distribution effect on three dimensional printed sand properties" (2018). *Dissertations and Theses @ UNI*. 534.
https://scholarworks.uni.edu/etd/534

This Open Access Thesis is brought to you for free and open access by the Student Work at UNI ScholarWorks. It has been accepted for inclusion in Dissertations and Theses @ UNI by an authorized administrator of UNI ScholarWorks. For more information, please contact scholarworks@uni.edu.

Offensive Materials Statement: Materials located in UNI ScholarWorks come from a broad range of sources and time periods. Some of these materials may contain offensive stereotypes, ideas, visuals, or language.

SAND DISTRIBUTION EFFECT ON THREE DIMENSIONAL PRINTED SAND PROPERTIES

An Abstract of a Thesis

Submitted

in Partial Fulfillment

of the Requirements for the Degree

Master of Science

Kip Woods

University of Northern Iowa

May 2018

ABSTRACT

The purpose of this study was to assess the performance characteristics of commercially available round grain silica sand for the use in three-dimensional sand printers. Two different average diameters were selected to examine the effects of screen distribution on printing performance; these diameters were 57-grain fineness number (GFN) and 70 GFN. These sands were a high purity round grain silica and had low trace contaminates, to reduce any possible influence from contaminates.

The resin system utilized in this investigation was a commercially available Furan resin system. Two test specimens were used in this study the American Foundry Society (AFS) tensile “dog bone” and 1” x 1.5” x 2” rectangle samples to calculate the printed part sand density. The resin content during the printing trials was adjusted by holding the resin droplet constant and changing the sand volume and the droplet to droplet distance. The cubic volume of sand is equivalent to the voxel size. The voxel size is determined by the resolution machine settings for the sand printer used in this investigation. Eight trials were printed with the four voxel sizes and repeated for the two sand GFNs. This was followed by a complete replication of the machine settings and sand types for a grand total of sixteen data sets.

Each trial consisted a total of thirty dog bones with ten placed parallel to the three Cartesian axes’ (X, Y, and Z). There were four density samples per axial direction for a total twelve samples per trial. The dog bone samples were evaluated on the mass,

tensile strength, scratch hardness, permeability, and loss of ignition (LOI) to determine resin content of the bonded sample.

The measured resin content on the bonded samples by LOI testing showed to be 0.97% to 2.02% based upon the sand voxel size. Analysis of Variance (ANOVA) was used to determine that there was no axial difference between the resin content of printed samples. The tensile strength results demonstrated that the GFN did impact the strength performance characteristics of the tested sands. The 57 GFN sand experienced a linear reduction of strength as the sand voxel size increased. The 70 GFN exhibited a unique profile for the middle voxel shapes as the tensile strength remained the same for two different resin levels of 1.5% and 1.3%. Both sand distributions experienced a reduction of Z-axial strength below 1% resin. The 70 GFN experienced a greater reduction of the Z-axial strength than the 57 GFN. This difference was attributed to the greater amount of grain to grain contact points within the 70 GFN sand.

The investigation confirmed that at the traditional Furan operating resin levels of 1.25% to 1.5% there was indeed a difference in physical properties between the two screen distributions for 3D printed sand (3DPS). Previously published studies for 3DPS utilized the manufacturer consumables and reported the physical properties. This investigation confirmed that a non-qualified sand will perform in 3DPS applications with the proper machine settings are utilized.

SAND DISTRIBUTION EFFECT ON THREE DIMENSIONAL PRINTED SAND PROPERTIES

A Thesis

Submitted

in Partial Fulfillment

of the Requirements for the Degree

Master of Science

Kip Woods

University of Northern Iowa

May 2018

This Study by: Kip Woods

Entitled: SAND DISTRIBUTION EFFECT ON THREE DIMENSIONAL PRINTED SAND PROPERTIES

has been approved as meeting the thesis requirement for the

Degree of Master of Science

_____	_____
Date	Dr. Scott Giese, Chair, Thesis Committee
_____	_____
Date	Dr. Mark Ecker, Thesis Committee Member
_____	_____
Date	Dr. Zhe Zhang, Thesis Committee Member
_____	_____
Date	Dr. Patrick Pease, Interim Dean, Graduate College

TABLE OF CONTENTS

LIST OF TABLES

LIST OF FIGURES

CHAPTER 1

INTRODUCTION

The process of casting metal has been around since humanity progressed from the stone age into the bronze age. One of the earliest intact castings, discovered in Baluchistan, Pakistan, has been estimated to be roughly 6,000 years old and this casting is shown in Figure 1 (Thoury et al., 2016). The medallion was made using lost wax, which is a separate casting method from sand casting. Both methods are similar ithat they use a pattern to create the void space into which the liquid metal will be poured to create the final casting geometry.

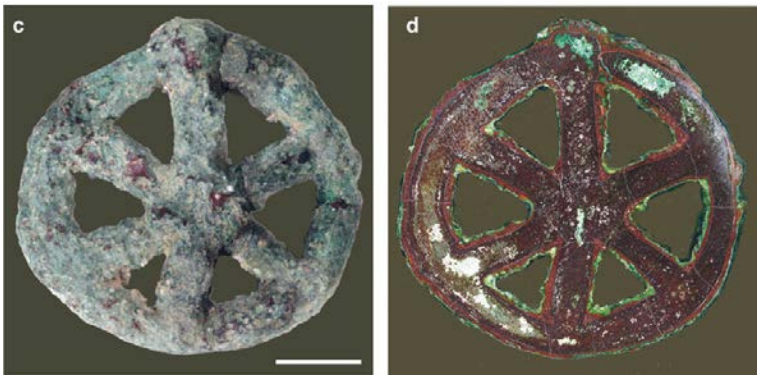

Figure 1. An early example of lost wax copper amulet (c)exterior visual image (d)interior cross-sectional image using dark-field imaging.
Reproduced from Thoury et al., 2016

Traditional sand casting utilizes a pattern to create an open void space for the liquid metal to flow into during the casting process. It is during the process of creating the mold void space that many design constraints are imposed upon the final part

geometry. The biggest constraint is the requirement of proper draft angle and selection of the parting lines during the mold making process as demonstrated in Figure 2.

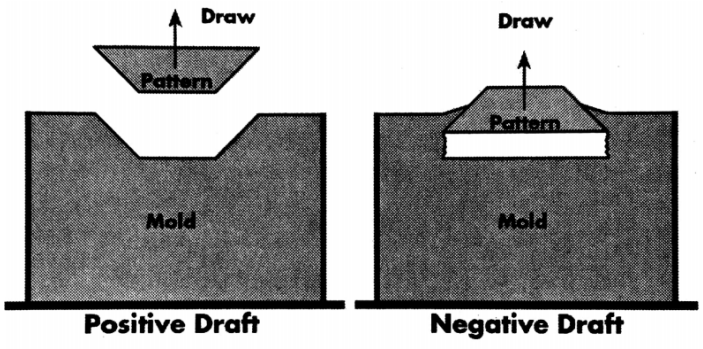

Figure 2. Negative draft makes removal of the pattern from molds problematic. Reproduced from Schleg 2003

The level of complexity that three-dimensional sand printing (3DSP) allows a part designer is a monumental shift in the freedom of design. Figure 3 demonstrates a traditional sand core that required eight individual pieces that were assembled into the desired final geometry for the core assembly. Three dimensional printed sand (3DPS) cores in this example reduce an eight piece assembly into one piece printed core. The largest benefit is the removal of stacking tolerances in the assembly and reduction of hard tooling to produce the individual sub components. This reduction of hard tooling is the largest cost savings for low quantity complex casting.

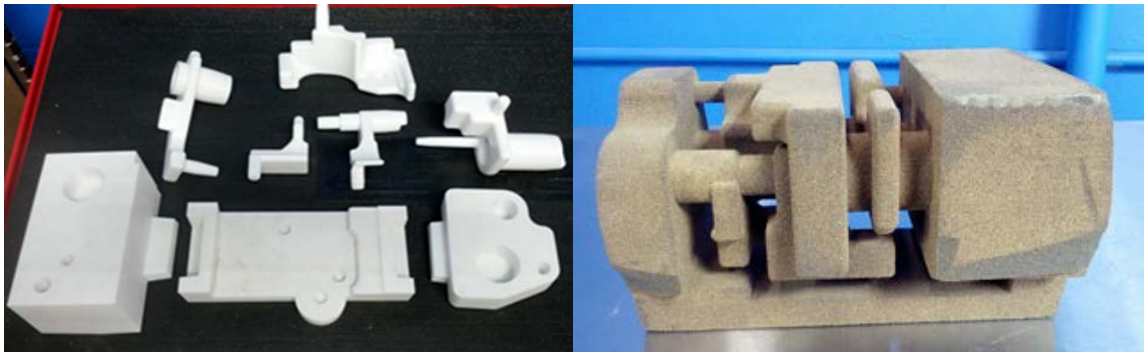

Figure 3. Left image is a plastic demonstration model of an eight piece internal core set. Right image is a single piece 3D print sand core(3DPS).
Reproduced from Woods & Ravi, 2015

3DSP removes the requirement of no negative draft or undercuts by selectively chemically bonding the geometry one layer at a time as shown in Figure 4. The process of chemically bonded sand involves the use of two chemicals combined in the medium of sand that over time will become rigid (Schleg 2003). This process can also be additionally referred to as a No Bake molding method (Sahoo & Sahu, 2014).

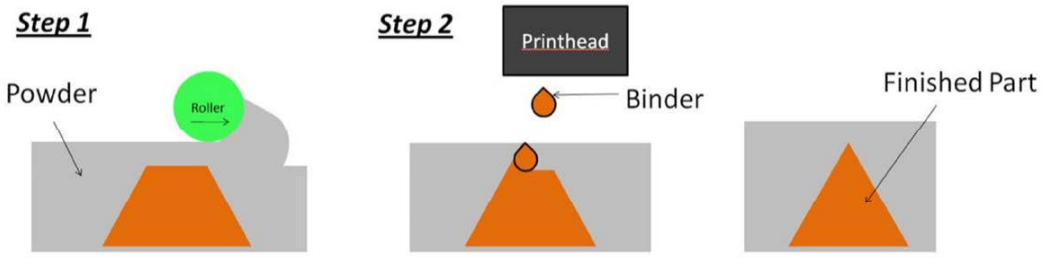

Figure 4. Process overview of 3DPS.
Reproduced from Snelling et al., 2013

The most widely used resin system for 3D sand printers is the Furan resin system. In the traditional no bake Furan the typical resin percentage is based on sand

weight (BOS). The typical resin content is 0.8 to 1.2% BOS and the acid catalyst level is typically 20 – 50% based on the binder weight (BOB) or based on resin weight (BOR; HA International LLC. 2004). 3DSP differ when compared to traditional molding operations such that the acid catalyst level is based as weight percentage of the sand batch being mixed.

Similar to paper printers requiring specific ink, most sand printer manufacturers require the use of qualified consumables. The consumables used by a 3DSP are the sand aggregate, resin, and the acid catalyst for a Furan printer. The largest material consumable used in the 3DSP process is the sand aggregate. The commercially available industrial sand printers require 5,000 to 23,000 lbs of silica sand for each printing job dependent upon build volume of the specific sand printer(ExOne 2012; Voxeljet 2016). The focus of this research will be on commercially available sand aggregates that are currently already used in traditional molding processes. Since traditional foundries already have silica sand in use in their foundries, it would drastically reduce the cost of operation for the 3DSP printer if traditional foundry sand could be used for 3DPS molds and cores without a reduction in the physical properties of the bonded sand.

Statement of the Problem

What is the effect of sand distribution and grain fineness number (GFN) on the physical properties of three-dimensional printed sand? What are the physical properties of 3DPS using traditional foundry silica sand?

Statement of Purpose

The purpose of this research is to understand better how the sand distribution and GFN will affect the overall physical properties of the bonded sand. Given that sand is the largest consumable for the 3D sand printing process, if an alternative source of commercially available sand could be found, this would provide the foundry industry with an alternative source for sand aggregates to be used in 3D sand printers.

Purpose of the Study

The purpose of this study is to provide research methodology for the evaluation of alternative sand aggregates for use in 3D sand printers.

Statement of Need and Justification

The current state of sand consumables for three-dimensional sand printers is only the sands qualified by the manufacturers of the three-dimensional sand printers can be used. This artificially creates a market with no price competition and results in a higher consumable price for those utilizing 3DPS in the foundry industry. This research would allow the ability for traditional sand suppliers to provide sands to 3DPS users thereby bringing back open market competition to the foundry industry.

Hypothesis and Research Questions

How does screen distribution affect the physical properties of 3DPS?

1. What screen distribution is acceptable for 3DPS physical properties?

2. Does the number of retained screens affect physical properties in 3DPS?

3. Does the printed density change based on the number of retained screens?

Assumptions

The proposed research shall be completed using a small capacity sand printer. This machine is assumed to be a representative model for 3D sand printers utilized by the sand printing industry. The sand aggregate used for this research is assumed to be a representative sample of the commercially available sand. The Furan and acid catalyst for this research is assumed to be a representative sample of the commercially available resin system.

Limitations

Due to the limited amount of published research concerning screen distributions for three-dimensional printing, the testing proposed is only applicable for round grain silica sands, and from a St. Peters deposit in Illinois limited to the Furan resin system. Due to the costs associated with consumables only two sand types will be tested a 57 GFN and a 70 GFN. The resin content will be tested at four different levels.

Definition of Terms

Binder — The chemical that is printed or mixed into sand to bond into a rigid structure.

Chemically Bonded Sand — sand that is held together using a chemical binder.

Core — A sand piece that makes up the internal and external sections of a metal casting.

Fire or Firing — Refers to when a piezoelectric element is actuated to release binder or fluid, also known as spitting.

Furan — A resin system utilized in the foundry industry that is a two-part system consisting of an acid catalyst and furfuryl alcohol.

Foundry — A workshop or factory for casting metal.

Inkjet — A term from the ink printing industry for a method of printing.

GFN — American Foundry Society Grain Fineness Number is the computed overall average diameter of a sand distribution also known as AFS GFN or GFN for short.

Loss on Ignition — The weight loss of a molding material after going through a thermal heating cycle at 1800°F for two hours to burn off any binder or volatile organic compound(VOC) on the sand aggregate.

Jets — the number of openings within a print head.

Mass Drop —A calibration test for drop on demand print heads that measures the total mass released for a set number of firings.

Mesh Size — numer of openings per linear inch for a sand screen that is used in determining the particle size distribution of granular material.

Mold — Refers to the sand structure that creates the exterior shapes of a casting

Nozzle — The opening in the printhead where binder or resin is released.

Permeability — The property of mold material to allow passage of mold/core gases during the pouring of molten metal.

Phenolic Urethane No Bake — A resin binder system that is utilized in the foundry industry.

Purging — The process of releasing binder with the purpose of cleaning the nozzles.

Resin — A chemical mixed with foundry sand to create molds or cores. In the case of Furan an acid catalyst is required within the sand for a proper reaction.

Scratch Hardness — A test method for determining the bonded sand structure resistance to scratches and abrasion damages.

Screen — Refers to the pore opening in the metal mesh at which a sand grain is captured and retained.

Screen Distribution — A method of displaying the individual screen profile of the sand aggregate.

Test Pattern — a printed shape for referencing purposes.

Tensile Strength — The resistance of a material to tension forces.

Transverse Strength — The property of a mold material during a 2 point load bending test.

Voxel — The geometric cubic volume of the three printer axis resolutions specifically X, Y and Z-Resolution.

X-Resolution — Printer machine setting to control the distance between resin droplets, also denoted xres and X_R.

Y-Resolution — The distance between print head nozzles also denoted yres and Y_R.

Z-Resolution — The sand layer thickness being printed also denoted zres and Z_R.

CHAPTER 2

REVIEW OF LITERATURE

Screen Distribution and Grain Fineness Number

Before a discussion concerning the physical properties of traditional No-Bake Foundry and differences from the 3DSP process can begin, a background understanding of how the foundry industry categorizes differences in sand aggregates must occur. Foundry sands are not comprised of a single uniform grain diameter. The cost associated with a single diameter sand would be exorbitantly expense. Therefore, no foundry uses mono diameter sands. Foundry sands are generally comprised of many different grain diameters and can also be referred to as an aggregate. Beginning in 1944 the American Foundry Association (AFA) began a tentative standard for the grain distribution of a sand (Booth & Sanders, 1954). This research was the precursor to the current standard utilized by foundry industry today.

The current foundry standard is the American Foundry Society (AFS) grain fineness number (GFN). Table 1 demonstrates the calculation of the GFN which determines the overall average grain diameter for the sand. When a sand is referred to as a two, three, or four screen sand this means 10% or greater is retained on a sieve/screen. In the Table 1 example below this sand would be a four screen sand with an GFN of 62.

Table 1. Example calculation of AFS GFN 1106-12-S and retained screens. Reproduced from AFS Mold and Core Test Handbook 2015

ASTME-11 Sieve Size	Percent Retained on Sieve	Multiplier to Calculate GFN	Product
6	0	0.03	0
12	0	0.05	0
20	0	0.1	0
30	2	0.2	0.4
40	2.2	0.3	0.66
50	14.4	0.4	5.76
70	34	0.5	17
100	32.7	0.7	22.89
140	13.2	1	13.2
200	1.5	1.4	2.1
270	0	2	0
Pan	0	3	0
Total	100	N/A	62

The shortcoming of describing a sand only by the GFN is that it does not fully describe the distribution profile of the sand. Figure 5 demonstrates two screen and three screen sand's with the same GFN but completely different distribution profiles. The two screen consists of a bi-nodal distribution while the three screen is a normal distribution, yet they both generate the same average grain diameter.

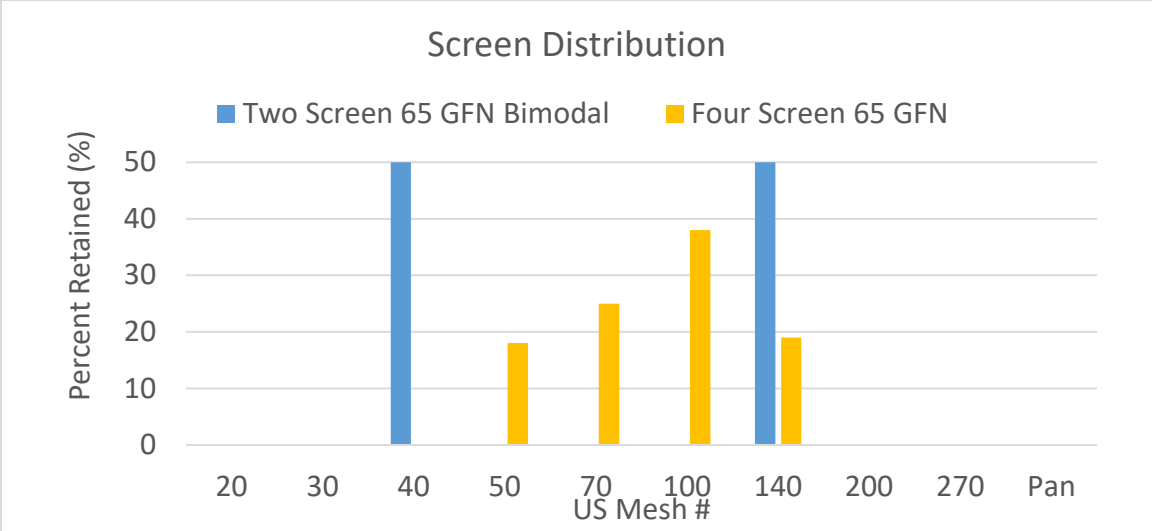

Figure 5. A theoretical example of constant GFN different screens, and distribution profile sands.

Influences of Screen Distribution Traditional Molding Methods

The impact of different screen distributions on the compaction properties of foundry sands was examined by Thiel, Ziegler, Dziekonski, and Joyce in 2007. The loose density of a sand is determined by placing a known mass gently into a graduated cylinder and recording the volume. Loose density and bulk density are interchange terms. The tapped density of a sand is determined by using a loose density specimen and gently tapping the side of the graduated cylinder until the sand volume stabilizes and tapping does not reduce the height of the sand specimen any further. Thiel al et. noted that a bi-nodal sand distribution resulted in an increased tapped sand density as shown in Table 2 compared to the other tested screen distribution profiles.

Table 2. Densities of modified screen distributions
Reproduced from Thiel et al., 2007

	Control 55 GFN	Skew Right 53.3 GFN	Skew Left 44.1 GFN	Bi-modal 45.2 GFN	Flat Dist 50.26 GFN	Narrow Dist 55 GFN
Loose density lbs/ft^3	95.21	102.53	102.36	102.25	99.97	96.56
Tapped Density lbs/ft^3	108.45	106.01	104.07	123.5	111.34	103.96

Grain Shape of Sand

Beyond the distribution of the grain diameters the grain shape is also a key consideration for foundry sands. The foundry industry classifies four major grain shapes: rounded, subangular, angular, and compound (Schleg, 2003) as shown in Figure 6. The grain shape factor has been determined for rounded at 1.2, subangular 1.4, and angular 1.6 (AFS Mold and Core Test Handbook, 2015).

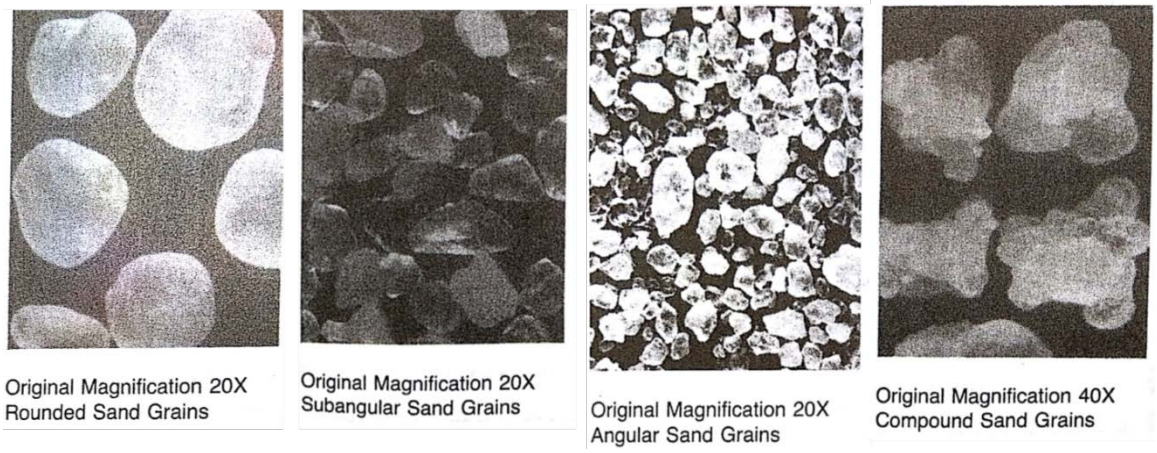

Figure 6. Sand grain shape classification.
Reproduced from AFS Mold and Core Test Handbook 2015

Surface Area of Sand

Another consideration of the sand aggregate is the surface area of the sand which can be calculated using the AFS GFN, grain shape, and grain type. The grain type has a determined factor multiple based upon whether the grain type is silica, olivine, chromite, or zircon sand. AFS 1109-12-S details the full procedure for the determination of calculated surface. Table 3 displays the surface area product of the sieve screens and the grain shape factor for silica sand on the previously used example four screen 62 GFN silica sand. The benefit of analyzing sand using the surface area is that it provides a better representation of the sand aggregate as whole because the GFN, grain shape, and grain type are all incorporated into the final value of 195 cm^2/g. Green sand molding has observed increases surface area requires greater additions of water to clay sand mixtures (Sanders & Doelman, 1968).

Table 3. Example calculation of calculated surface area S based on grain shape and AFS GFN 1109-12-S and retained screens. Reproduced from AFS Mold and Core Test Handbook 2015

Calculated Surface Area 62 GFN Silica Sand			
Sieve Size	% Retained	Surface Area factor	Surface Area product
20	0.00	20	0.000
30	2.00	40	0.800
40	2.20	60	1.320
50	14.40	90	12.960
70	34.00	130	44.200
100	32.70	190	62.130
140	13.20	270	35.640
200	1.50	400	6.000
270	0.00	600	0.000
Pan	0.00	900	0.000
Total	100.00		
		SA Sum	163.050
		Grain Shape Factor	1.200
		Calculated Surface Area (cm^2/g)	195.660

Traditional No-Bake Furan Acid Catalyst Type and Amount

Now with a foundational understanding of sand aggregate, characteristics in place the Furan resin system can be further explained. In traditional No-Bake mixing operations both the acid catalyst and the furan resin are both feed into a continuous sand mixer. The continuous mixer allows the homogenous coating of the grains where the furan and acid catalyst are mixed together. The ratio of resin to acid catalyst is dependent upon specific molding application, but generally the resin is applied 0.8 – 1.2% based on sand weight (BOS). While the acid catalyst is applied typically from 20 – 50% based on binder weight (BOB) or based on resin weight (BOR; H.A. International 2004).

The acid type and the amount of catalyst present directly affects the 24-hour strength, and rate of curing for the bonded sand as shown in Figure 7 (Nelson, 1973). In high production environments the rate of curing must be balanced with the desired 24-hour tensile strength requirements and provide sufficient initial strengths for removal from pattern box. In the example as shown in Figure 7, the Methanol-Toluenesulfonic acid the curing rate and 24-hour tensile strength is greater than of phosphoric acid catalyst.

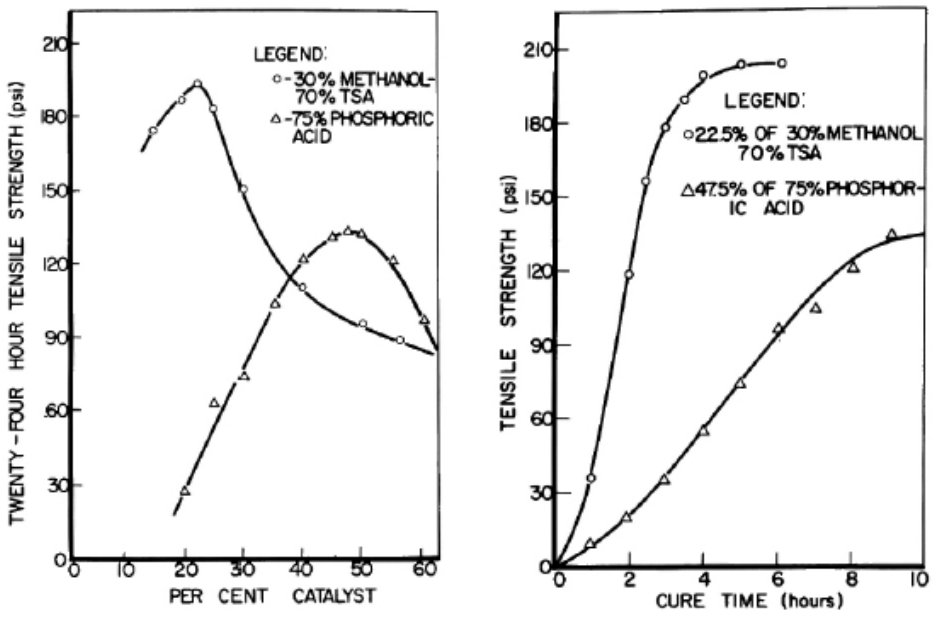

Figure 7. Left figure how acid catalyst type and amount present determines final tensile strength. Right figure how acid catalyst type and amount influence curing tensile. Reproduced from Nelson, 1973

Properties of Traditional No-Bake Furan and Sand Aggregate Performance

The identification of potential sand aggregates that would be suitable for 3DSP has been an area of interest for the sand casting industry. A study published in 2017 by Thiel, Ravi, and Bryant demonstrated using traditional hand rammed tensile specimens the suitability of alternative sand aggregates with the Furan resin system. The results from this investigation are summarized in Table 4. There was wide varied of sand aggregate tested with a large difference in GFN, and grain shape. This research demonstrated the ability of the Furan resin system to bond a wide varied of sand types and provides a reference point for the tensile strength of traditionally produced tensile specimens.

Table 4. Furan No-Bake with TSA acid catalyst average tensile strength with various sand aggregates.
Reproduced from Thiel et al., 2017

Sample	Grain Shape	AFS-GFN	Surface area (cm2/g)	Bulk density (g/cc)	Tapped density (g/cc)	Tensile Strength (PSI)	Binder Content (%)
1	Rounded	81.9	270.68	1.554	1.769	141	1
2	Rounded	54.87	142	1.819	2.070	124.8	2.5
3	Rounded	64.56	252.69	1.424	1.694	118.5	2
4	Rounded	89.3	94.17	2.694	3.015	148.2	1.25
5	Rounded	92.26	238.78	1.839	2.007	107.3	1.5
6	Rounded	66.47	183.1	1.422	1.723	103.2	2.5
7	Angular	96.8	437.918	0.989	1.256	28.2	1
8	Rounded	66.52	183.832	1.516	1.673	53.6	1
9	Rounded	79.82	184.983	1.445	1.620	73.7	1
10	Subangular	102.49	265.56	1.434	1.623	62.3	1
11	Rounded	80.42	152.55	1.410	1.510	134.4	1

3D Sand Printer Technology Difference from Traditional Furan Molding

The most fundamental difference between traditional molding process and 3D sand printing with respective to a Furan process is the individual printing a single layer at a time. Due to the need of selectively bonding the required geometry this creates an process where only the sand aggregate has been coated with the acid catalyst and is spread across the build bed. Figure 8 shows a 3D sand printer spreading a new layer of precoated silica sand. The apparatus in the right image of Figure 7 is called a recoater (Voxeljet 2016). The amount of sand that egresses the recoater is controlled by the vibrational frequency and the gap opening.

There is concern regarding vibrational compaction methods for sand aggregates from early research. Pedicini (1958) concluded that sand distributions with coarse grains would benefit from vibrational compaction greater than fine grains. However, Heine and Seaton noted that excess vibration would eventually lead to a reduction in packing density (1958). Seaton later confirmed that vibrational compaction is the most energy efficient method for sand compaction (Seaton 1960). Density is a major molding concern since mold and core density issues are the root cause for most metal penetration issues (Scott, Easterly, Lodge, & Blackburn 2004).

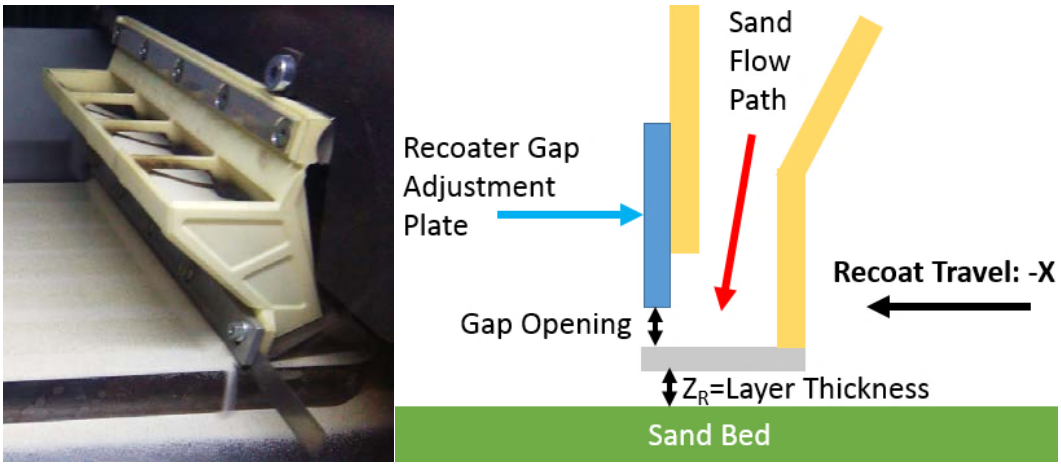

Figure 8. Left image: Recoater spreading precoated silica sand in an 3D Sand Printer. Right image: Schematic diagram of the recoater and gap opening.

Capillary Forces between Grains

One unique aspect of the 3DPS process is the repeated spreading of sand one layer at a time. Since the sand has been precoated with an acid catalyst in the case of a Furan resin system, this introduces capillary forces between the liquid bridge and the

sand grains. The initial understanding of capillary forces begins with capillary pressure (P_C) as shown in Equation 1 where r_C is the radius of the capillary tube, σ is the interfacial tension, and θ is the wetting angle of the liquid on the surface of the capillary (Djebbar & Donaldson, 2012).

$$P_C = \frac{2\,\sigma \cos\theta}{r_c} \quad (1)$$

Anyone that has been present on a sand beach during a rainy day has observed this clumping of the sand as the rain initially begins, but if you look to where the sand is already wet from the tide, the droplets are quickly wicked into the sand. Harireche, Farmarzi, and Alani (2013) examined how the capillary forces between a polydispersive particles measure compared to the various ratios of the diameters as shown in Figure 9. Polydispersive means diameters of different sizes. The capillary force was the greatest when the grain diameters were equal and as disparity between grains was the largest the capillary force was the lowest. Foundry sands are essentially polydispersive systems just not perfectly spherical in the grain shape.

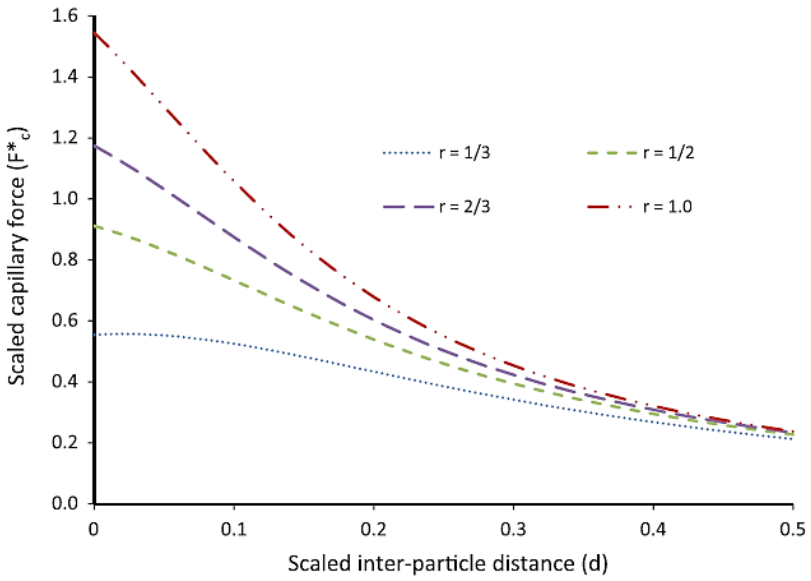

Figure 9. Capillary force (F^*_C) over inter-particle distance (d) r = ratio of grain sizes (small grains/ large grain, and equal grain size)
Reproduced from Harireche et al., 2013

Published 3DPS Sand Research

Tensile Strength and Bending Strength

There have been a number of investigations in the physical properties of 3DPS using the manufacturers Furan resin system and the manufacturer approved silica sand. Snelling et al., completed an investigation in 2013 comparing the binder burnout and bonding characteristics between 3DPS Furan and traditional foundry resin systems. Coniglio, Sivarupan, and Mansori examined the anisotropic properties of 3DPS (2018). Hackney and Wooldridge examined the process capabilities of 3DPS for a production sand molding replacement method (2017). Nyembwe, Mashila, Tonder, Beer, and

Gonya investigated the physical properties of 3DSP (2016). These investigations recorded the tensile strength or the 3-point (3PT) bending strength of the bonded samples. The results from these investigations will provide a baseline for the manufacturer qualified resin and silica sand properties. The tensile and 3 PT bend strength are shown in Table 5 along with the machine type and machine manufacturer. The reported tensile strengths ranged from 108 to 192 PSI.

Table 5. Published investigations into the 3DPS Furan resin system with silica sand and the observed bonding strengths with failure mode.

Source	Test Specimen	Failure Mode	Value	Unit	Machine Type	Converted (PSI)
Snelling et al., 2013	AFS 3342-00-3 "Dog Bone"	Tensile	1324.931	kPa	ExOne S-Max	192
Coniglio et al., 2018	22.4 x 22.4 x 172 (mm)	3 PT Bend	1.12 to 2.7	MPa	ExOne S-Print	166 to 391
Hackney & Wooldridge 2017	ISO/CD 6892-1	Tensile	11	kN	ExOne S-Max	N/A
Nyembwe et al., 2016	AFS 3342-00-3 "Dog Bone"	Tensile	75	N/cm2	Voxeljet VX1000	108
Nyembwe et al., 2016	1 x 1 x 8"	3 PT Bend	235	N/cm2	Voxeljet VX1000	340

Printed Sand Density

One key commonality between the published 3DPS data was that the bonded sand density was much lower than the observed tapped density of the silica sand as shown in Table 6. In the research completed by Nyembwe et al., (2016) they utilized the same consumables as in the 3DSP process but handrammed specimens for comparison to the traditional molding method. Nyembwe et al., (2016) observed that the

handrammed density was between 1.51 to 1.55 g/cm^3 compared to the 1.35 g/cm^3 of the 3DPS samples. The samples produced by 3D sand printer exhibited a much lower bonded sand density. The authors attributed this reduction in density due to the lower compression forces present during the recoating process comparative to the forces present during traditionally handrammed molding method.

Table 6. Published investigations into the 3DPS Furan resin system with silica sand and printed sand density.

Source	Density	Units
Nyembwe et al., 2016	1.35	g/cm3
Hackney & Wooldridge 2017	1.435 to 1.495	g/cm3
Coniglio et al., 2018	1.331	g/cm3

Compaction Characteristics of Particles

The density reduction of the 3DPS warranted further investigation into the nature of particle packing characteristics. The powder metallurgy industry, road compaction, and many other industries have long studied this phenomenon. The mathematical analysis of uniform sphere packing states was examined by Smith, Foote, and Busang in 1929 their research created the term “coordination number” which is still used today to describe the grain to grain contact of spherical systems.

One of the initial early methods of examining real-world packed sands involved compacting the sand and filling the interval voids with a polyester-resin, taking great care not to disturb the packed sand(Oda , 1972). Once the resin was fully set, this rigid

sample was cut into thin wafers and examined under the an optical microscope to better understand the packing characteristics of granular materials. This thin rigid sample was called a sand fabric. Much of the early real world examinations of sands were conducted with this method to determine the coordination number(CN) in real-world trials(Oda 1972). The CN is how many other grains can a single grain can touch for a sand aggregate. The mathematical analysis of the CN of sand is still examined today with the benefit of computers and has moved to distributions beyond uniform and normal distributions as shown in Figure 10. The CN increases as the compressive loads (σ_Z) are applied during computer modeled discrete element method (DEM) analysis. The particles eventually reach a maximum compaction level and once this compacted state is reached, it will remain constant until the grains themselves start to fracture under the compressive load. Regardless of the underlying distribution, all systems experienced an increased CN with increased packing structure.

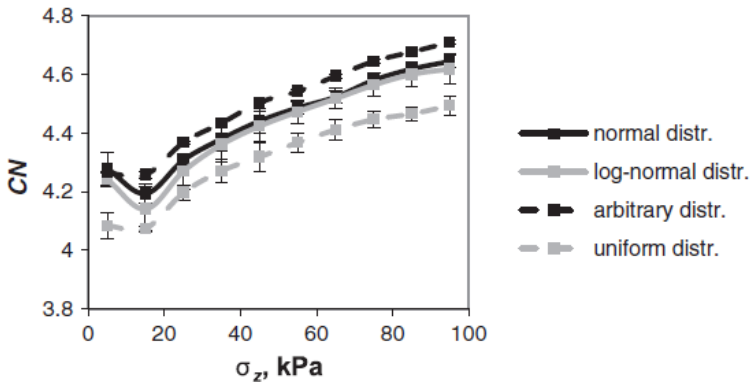

Figure 10. Discrete element method computation analysis of coordination (CN) under various compressive loads (σ_Z) of granular matter.
Reproduced from Wiacek & Molenda, 2014.

Pinson, Zou, Yu, Zulli, and McCarthy (1998) examined how CN changed in a series of trials using single diameter, two diameter uniformed spherical steel ball bearings mixtures. Three different diameters were tested with a different ratio of large to small diameters as shown in Table 7 for six total different mixtures. The research showed that the average CN was roughly 6 for the spherical steel ball bearings.

Table 7. Coordination number of Binary packed spheres.
Reproduced from Pinson et al., 1998

	Volume fractions (%)				
Mixture	25.4 mm	12.7 mm	6.4 mm	Overall mean coordination number	Porosity
1	—	100	—	6.240	0.406
2	28	72	—	6.442	0.388
3	72	28	—	6.199	0.379
4	28	—	72	6.158	0.345
5	50	—	50	6.428	0.308
6	72	—	28	6.275	0.299

The investigation of the CN for sub-angular and angular sands was conducted by Celauro, Ziccarelli, Parla, and Valore in 2014. Their research consisted of automated optical analysis of the sand samples. The CN with the frequency count can be viewed in Figure 11. The authors stated if this analysis was conducted in the three dimensions the CN value would have been higher than the peak CN of 3. The top three observed CN was four, five, and six in order of largest to smallest.

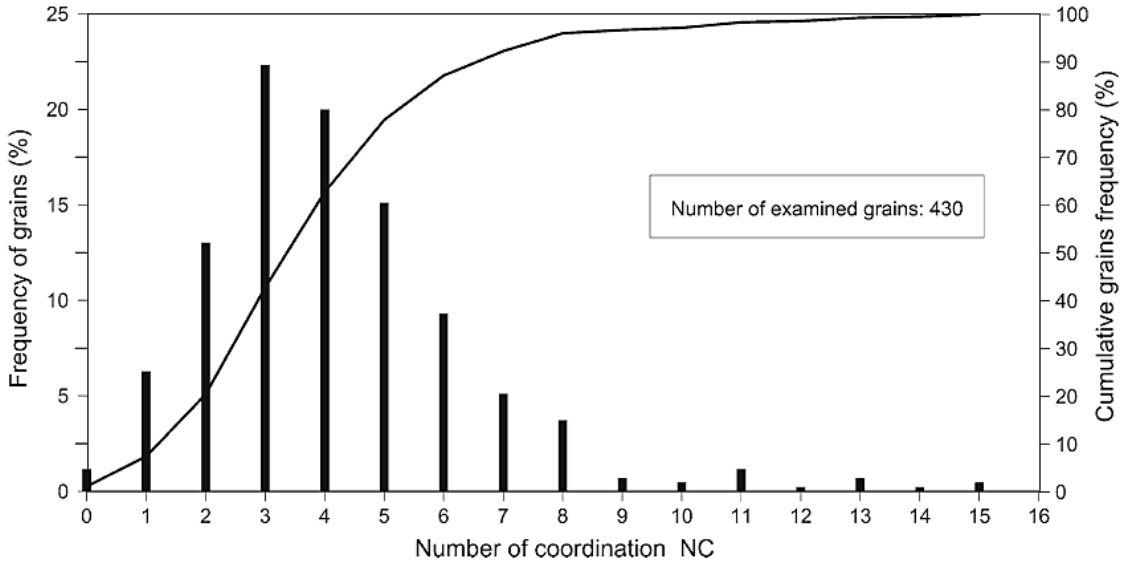

Figure 11. Numidian Flysch formation sand coordination number cumulative histogram. Reproduced from Celauro et al., 2014

Coordinate Number and Resin Volume at Contact Points

The literaure review confirmed that the generally accepted coorindate number of a properly compacted sand particle system was 6. Nagai et al., (2016) examined a resin coated transverse specimen using x-ray computed tomography (CT). Resin coated sand is a sand aggregate that is coated with heat cured resin system that fully encapsulates the sand grain with resin. The authors were able to map the open void space between the sand grains and determined the grain to grain contacts per unit volume. The first step of their research was to calculate based upon the GFN what would be the total number of grain to grain contact points with a CN of 6 as shown in Table 8. The total number of grain to grain contact points increased as the GFN increased.

Table 8. The calculated number of particles and particle points of contact per unit cubic Millimeter based on AFS GFN.
Reproduced from Nagai et al., 2016

	Natural Silica Sand 1	Natural Silica Sand 2	Natural Silica Sand 3	Natural silica sand polished	reclaim sand	Natural silica sand high purity 1	Natural silica sand high purity 2	Average
AFS GFN	49.3	53.8	61	63.2	64.9	60.5	62.1	59.3
Sieve mesh opening, mm	0.318	0.29	0.255	0.245	0.239	0.257	0.25	0.265
Sieve offset (x1.25),mm	0.398	0.363	0.318	0.307	0.298	0.321	0.312	0.331
Particle volume at sphericity, mm^3/particles	0.0329	0.025	0.0169	0.0151	0.0139	0.0173	0.016	0.0196
Number of particles at 60% filling rate particles/mm^3	18.2	24	35.5	39.7	43.2	64.6	37.6	33.3
Number of particle points of contact at coordination number of 6, points/mm^3	55	72	107	119	129	104	113	100

Nagai and associates than determined the experimental values of the CT scanned resin coated sand transverse bars. They determined a threshold limit to remove the noise of the CT scanning method. The results of their research are shown in Table 9. The key area of interest was that the sand type with the highest transverse strength of 131.2 also had the largest number of sand-grain points per unit volume. Additionally, this sand also had the largest percent of resin residing at the sand-grain points. Essentially, a chemically bonded or resin coated sand system is held together by the resin to grain contact points. If there is a proper resin volume at the grain to grain contact points, than a strong sand system is created.

Table 9. X-Ray Computed Tomography results of shell molds.
Reproduced from Nagai et al., 2016

	Natural Silica Sand 1	Natural Silica Sand 2	Natural Silica Sand 3	Natural silica sand polished	reclaim sand	Natural silica sand high purity 1	Natural silica sand high purity 2
Transverse Strength	45.1	34.9	53.5	71.6	57.6	108.2	131.2
	Filtering under 3.17 E-05 mm^3 (Noise removal)						
Volume at sand-grain points of contact per cubic millimeter, mm^3	0.00504	0.00505	0.00627	0.00749	0.00735	0.00853	0.01035
Number of sand-grain points of contact per unit volume, points/mm^3	63	64	87	106	109	122	150
Porosity, vol%	40.6	41.4	41.6	40.9	38.6	41.1	35.7
Resin content, vol%	3.56	3.48	3.54	3.59	3.66	3.57	3.93
Volume at sand-grain points of contact(resin content at points per cubic millimeter), vol % (mm^3)	0.5	0.5	0.63	0.75	0.73	0.85	1.04
Resin ration sand-grain points of contact, %	14.1	14.5	17.7	20.9	20.1	23.9	26.3

Resin Content of Printed Sand

Traditional molding has the benefit of bonding the complete pattern box of sand whereas 3DSP process is selectively bonding the individual printed parts. Selectively bonding makes determining the resin content of the printed sand a much different approach than traditional molding operations. In traditional molding the operator measures the amount of sand dispensed by the mixer for a set duration and the process is repeated for the chemical resin. The weight of resin divide by weight of sand yields the weight percent of resin to sand. For 3D sand printers the machine settings must be used to determine the resin content. Initial investigations were conducted to determine

what 3D sand printer machine settings would impact the resin content of the printed sand (Thiel et al, 2017). The two machine settings that contributed the most to resin content were the spacing between resin droplets controlled by the X-Resolution (X_R) and the sand layer thickness (Z_R) as shown in Figure 12.

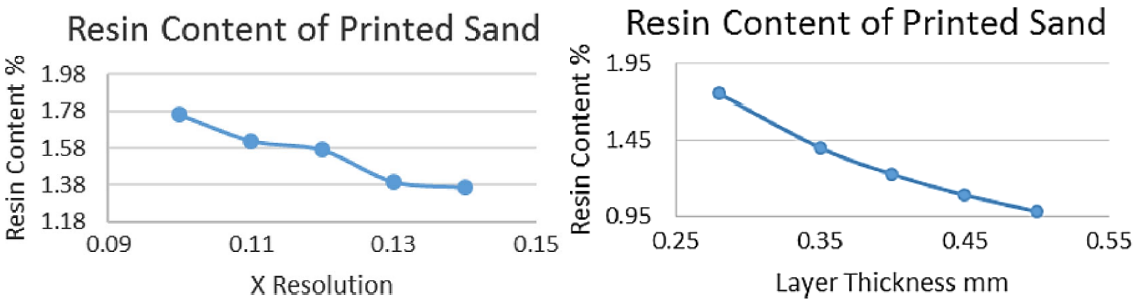

Figure 12. Observed resin content on 3DPS samples and machine settings that impacted the resin content.
Reproduced from Thiel et al., 2017

The contribution of X_R was observed that the lower the X_R the higher the resin content of the bonded sand. Figure 13 shows a theoretical fine resolution (lower) vs coarse (higher) X_R.

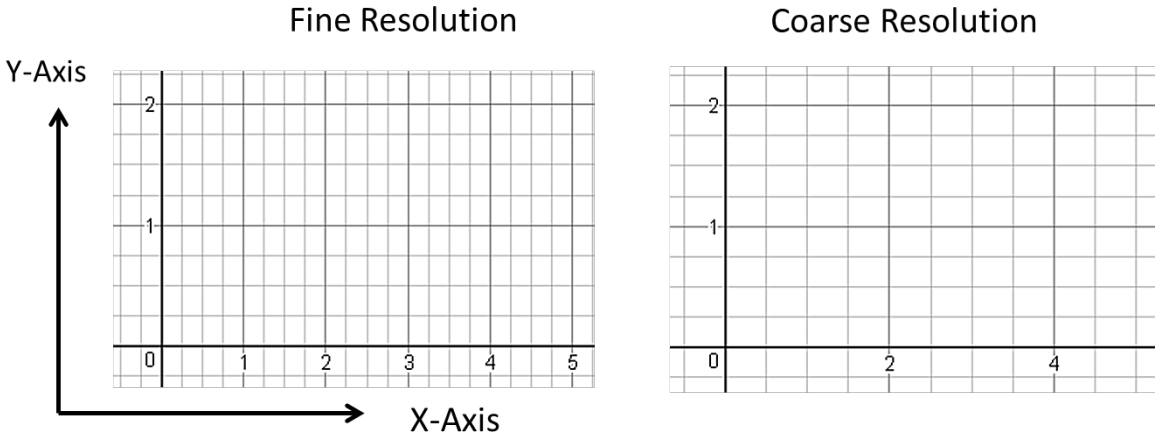

Figure 13. Graphical representation of different X-Resolutions.

The Y-Resolution (Y_R) is the spacing distance between the printhead nozzles in Y-Axis. The cubic volume of the X_R,Y_R, and Z_R creates a voxel. The resin is released one droplet per voxel. The individual droplet mass, printed sand density, part volume, and voxel size determines the resin content present on the printed sand(Woods, Richardson, & Trikha In Press). Equation 2 was used to determine the printed resin content ($P_{\%R}$) for 3DPS for Furan resin system is shown below. P_V is the part geometry volume, D_M is the individual droplet mass, and P_{SD} is the printed sand density of the aggregate.

$$P_{\%R} = \frac{\frac{P_V}{X_R * Y_R * Z_R} * D_M}{P_{SD} * P_V} * 100 \quad (2)$$

Analysis of Variance Overview

The statistical analysis method called analysis of variance was developed by Ronald Fisher, and the first application of this method was published in 1921. The use of ANOVA test method was detailed in his 1st edition book published in 1925 called

Statistical Methods for Research Workers, which is currently is in its 14th edition (Fisher, 1970). An example of a computerized application for ANOVA within the SAS/STAT(R) software is shown in Figure 14. 3DOK1 through 3D0K13 refer to individual data points with an associated Nitrogen level. This contains an example data set that will be used to explain the Tukey analysis of means.

```
title1 'Nitrogen Content of Red Clover Plants';
data Clover;
   input Strain $ Nitrogen @@;
   datalines;
3DOK1  19.4 3DOK1  32.6 3DOK1  27.0 3DOK1  32.1 3DOK1  33.0
3DOK5  17.7 3DOK5  24.8 3DOK5  27.9 3DOK5  25.2 3DOK5  24.3
3DOK4  17.0 3DOK4  19.4 3DOK4   9.1 3DOK4  11.9 3DOK4  15.8
3DOK7  20.7 3DOK7  21.0 3DOK7  20.5 3DOK7  18.8 3DOK7  18.6
3DOK13 14.3 3DOK13 14.4 3DOK13 11.8 3DOK13 11.6 3DOK13 14.2
COMPOS 17.3 COMPOS 19.4 COMPOS 19.1 COMPOS 16.9 COMPOS 20.8
;

proc anova data=Clover;
   class Strain;
   model Nitrogen = Strain;
   means Strain / tukey;
run;
```

Figure 14. Example code of ANOVA within SAS/STAT(R) software.
Reproduced from SAS/STAT(R) 9.22 User's Guide. (2018)
Retrieved from
https://support.sas.com/documentation/cdl/en/statug/63347/HTML/default/viewer.htm#statug_anova_sect027.htm

The output from an ANOVA can be adjusted using a specific analysis method. In the course of this investigation, Tukey was selected since all samples being compared are an equal number of data values (Ott & Longnecker, 2010). An example of the Tukey output can be viewed in Figure 15. In this example samples with the same letter grouping (A, B, C, etc) are not statistically different from each other. If a sample has a

lettering label that overlaps with a different letter these samples are not statistically different from each other, for example, 3DOK7, and COMPOS both have the B and C Tukey grouping. This means that these two samples are not statistically different. The only samples in this example that are statistically different would be 3DOK1 compared to 3DOK4 and 3DOK1 compared to 3DOK13. To reduce confusion for the ANOVA analysis conducted in this investigation. The alphabetic output A, B, C, etc have been replaced with Roman numerals I, II, III, etc to avoid confusion with the Series A and Series B trials.

Nitrogen Content of Red Clover Plants

The ANOVA Procedure

Tukey's Studentized Range (HSD) Test for Nitrogen

Alpha	0.05
Error Degrees of Freedom	24
Error Mean Square	11.78867
Critical Value of Studentized Range	4.37265
Minimum Significant Difference	6.7142

Means with the same letter are not significantly different.

Tukey Grouping		Mean	N	Strain
	A	28.820	5	3DOK1
	A			
B	A	23.980	5	3DOK5
B				
B	C	19.920	5	3DOK7
B	C			
B	C	18.700	5	COMPOS
	C			
	C	14.640	5	3DOK4
	C			
	C	13.260	5	3DOK13

Figure 15. Example Tukey ANOVA SAS/STAT(R) output.
Reproduced from SAS/STAT(R) 9.22 User's Guide. (2018) Retrieved from https://support.sas.com/documentation/cdl/en/statug/63347/HTML/default/viewer.htm#statug_anova_sect003.htm#statug.anova.anog1a

CHAPTER 3

RESEARCH METHODOLOGY

Sand Aggregate

The sand selected was commercially available round grain silica from the Illinois St. Peters deposit. A high purity silica was selected to reduce influence from trace minerals. Two three-screen sands, were selected a Wedron™ 530 (57 GFN) and a Wedron™ 510 (70 GFN) the complete screen distribution is shown Figure 16. While similar in distribution profile the mode for the 70 GFN is shifted one screen higher and the retained on the 140 and 200 mesh is double when compared to the 57 GFN. The calculated surface area for the 70 GFN at 152 cm^2/g vs the 57 GFN 121 cm^2/g.

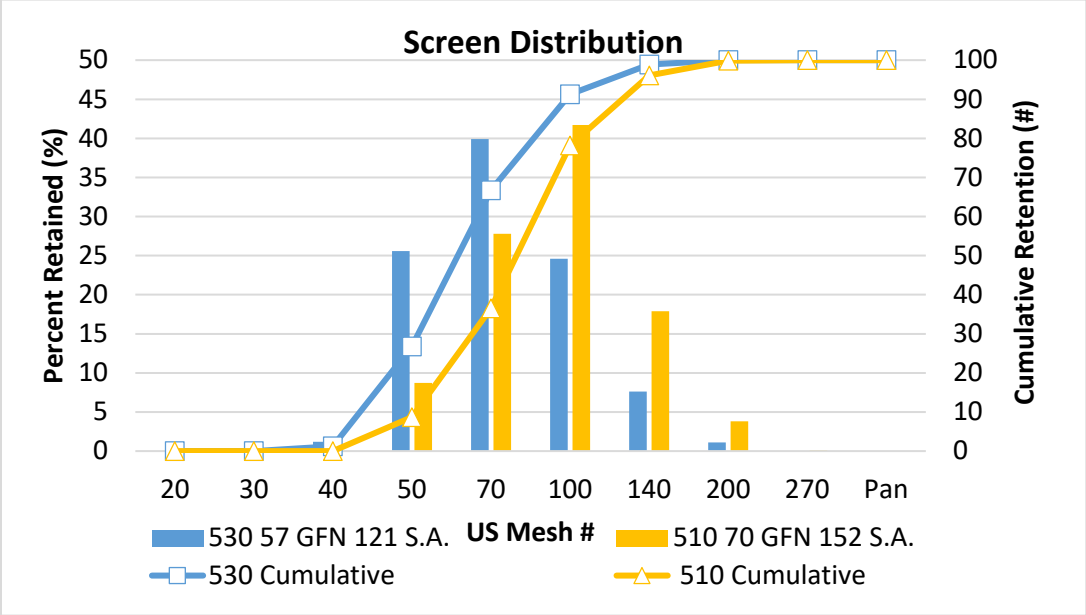

Figure 16. Sand Screen distribution for the Wedron 510 and 530 with the calculated surface area (S.A.). Reproduced from Fairmount Santrol 2014

Process Parameters and Estimated Resin Content

Two X-Resolutions (X_R) were selected 0.08 mm and 0.12 mm along with two Z-Resolutions (Z_R) were of 0.28 mm, the current industry standard, and a thicker sand layer of 0.39 mm. The estimated resin content using an assumed silica density of 1.3 g/cm^3 is shown in Table 10, this allowed for four different resin level to be analyzed.

Table 10. Calculation of estimated LOI for X_R and Z_R.

Estimated LOI	2.13	1.35	1.47	0.92
X-Res(mm)	0.08	0.12	0.08	0.12
Z-Res (mm)	0.28	0.28	0.39	0.39

Acid Coating of Sand

The furan resin binder system selected for study requires the sand aggregate to be precoated with the acid catalyst before loading into the VX200 sand printer, due to the printed having no sand mixing capabilities. The acid catalyst selected was TW40 (toluenesulphonic acid) from H.A. International LLC. The acid catalyst was applied at 0.2% based on total sand weight for all test series. The sand batches were weighed to 20.4±0.1 kgs, and the acid catalyst was weighed to 40.8±1 grams. Batches were mixed in a 50 lbs capacity Klien vibratory mixer for 60 seconds and loaded into the sand printer before the start of each trial.

Furan Binder System

The resin system used for all trials was H.A. International Enivroset 3D Jet Resin (H.A. International, 2014). This furan resin system is commercially available for 3D sand printing applications.

Machine Axis Definition

For this investigation, the machine operation will reference the Cartesian coordinate system of X, Y, and Z. The upper limit of each axis in the build box is displayed in Figure 17. The limitation in the Y and Z axis removed the selection of 1”x 1” x 8” transverse loading test standard for the investigation.

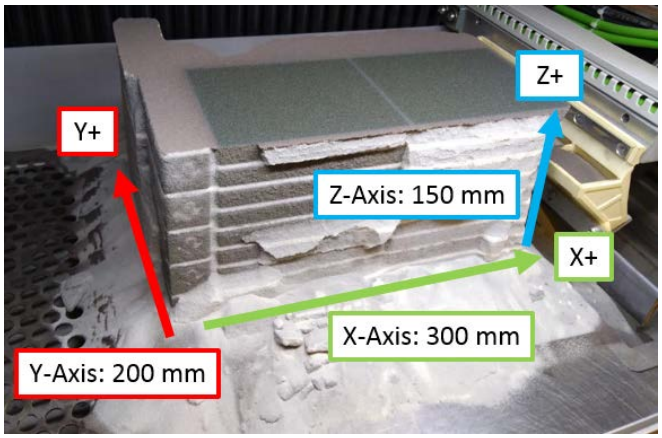

Figure 17. VX200 Machine axis orientation.

Build Box Layout

The tensile strength “dog bone” was selected as this allowed the ability to analyze the X, Y, Z-Axial strength characteristics during the same build conditions. The

dimensional specifications of the tensile specimen are shown in Figure 18. Additionally, this allowed the ability to place the samples throughout the build envelopment allowing randomization of part placement. The dog bone is an industry accepted test standard for the measurement of physical properties of chemically bonded sand.

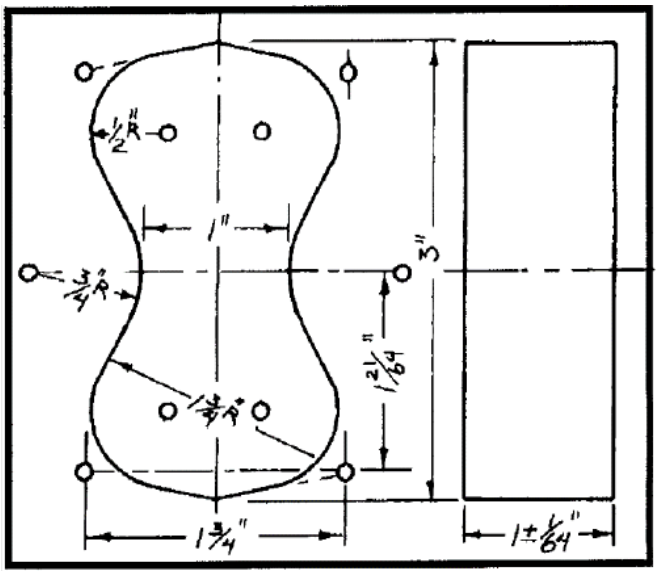

Figure 18. AFS Standard Tensile Specimen AFS 3342-00-3
Reproduced from AFS Mold and Core Handbook 2015

Figure 19 shows the printed layout in the build box, allowing for a total of ten dog bones per orientation for a grand total of thirty samples per test series. Four rectangles per orientation 1” x 1.5” x 2” will be printed to calculate the printed part density within the trial along the three-major axis, the 2” length being orientation parallel with the axis being evaluated. There will be a grand total of twelve density samples per test series.

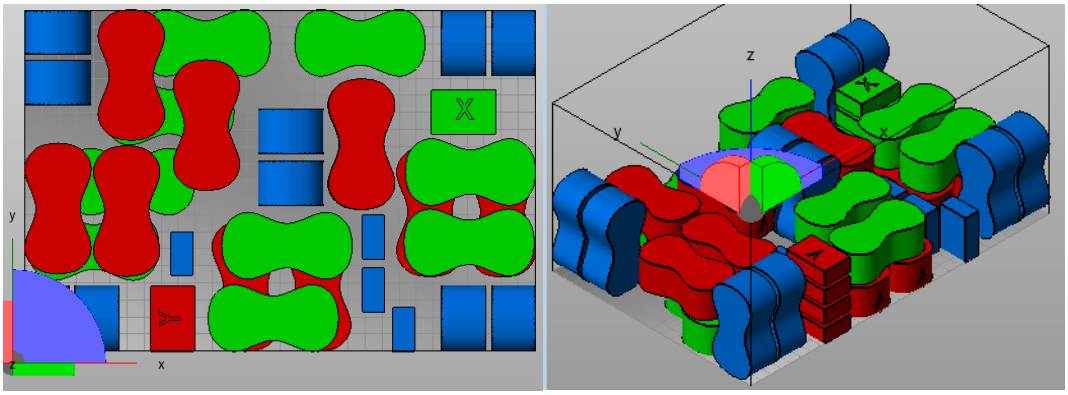

Figure 19. Printed Specimen layout 10 X, Y, Z Tensile samples, and 4 X,Y, Z Density rectangles. Green is for X-axis, Red is for Y-Axis, Blue is for Z-Axis orientations.

Test Matrix

The design of experiment for this investigation includes three factors: sand type, X_R, and Z_R. The combination of the three factors and two levels is shown in Table 11.

Design of Experiments

Table 11. Selected factors and tested levels with values

Factor A	Factor B	Factor C
Sand Type	X_R	Z_R
0 (70 GFN)	0 (0.08 mm)	0 (0.28 mm)
1 (57 GFN)	1 (0.12 mm)	1 (0.39 mm)

The printing trials were split into two series A and B. Series A consisted of series IDs 1A-8A and Series B consisted of test IDs 1B-8B as shown in Table 12. Series B was a duplicate of Series A outside of the inherit process variations.

Table 12. Printed test series overview.

	Factor	A	B	C
Print Order	Series ID	Sand (GFN)	XR (mm)	ZR (mm)
1	1A	57	0.08	0.28
2	2A	57	0.08	0.39
3	3A	57	0.12	0.28
4	4A	57	0.12	0.39
5	5A	70	0.08	0.28
6	6A	70	0.08	0.39
7	7A	70	0.12	0.28
8	8A	70	0.12	0.39
9	1B	57	0.08	0.28
10	2B	57	0.08	0.39
11	3B	57	0.12	0.28
12	4B	57	0.12	0.39
13	5B	70	0.08	0.28
14	6B	70	0.08	0.39
15	7B	70	0.12	0.28
16	8B	70	0.12	0.39

When the factor of sand type is ignored, and a comparison of equal machine settings is tabulated, Series 1A, 1B=5A, 5B, etc as shown in Table 13. Theoretically, if there are no machine variations and sand type has no impact on printed properties, these series should be statistically the same since the only parameter changing is the sand type.

Table 13. Equivalent machine and sand parameter comparison.

Series ID	Sand (GFN)	X_R (mm)	Z_R (mm)	Series ID	Sand (GFN)	X_R (mm)	Z_R (mm)
1A & 1B	57	0.08	0.28	5A & 5B	70	0.08	0.28
2A & 2B	57	0.08	0.39	6A & 6B	70	0.08	0.39
3A & 3B	57	0.12	0.28	7A & 7B	70	0.12	0.28
4A & 4B	57	0.12	0.39	8A & 8B	70	0.12	0.39

Voxel Size Chart

For the test series analyzed the voxel size is calculated as shown in Table 14. Voxel ID V1 is the smallest voxel at 0.0023 mm^3. From the perspective of V1 the volume, X_R, and Z_R percent changes are additionally calculated. The examination of V2 0.0032 mm and V3 0.0034 mm shows that they are within 8% of total volume of each other, but the aspect ratio of the voxel size is completely different. V2 is 39% taller in the Z-axis, while V3 is stretched 50% in the X-axis. V4 experiences both the X and Z-axis increases resulting in the largest voxel volume at 0.0048 mm^3.

Table 14. Voxel size comparison chart and aspect changes.
Note Y_R was constant at 0.1016 mm for all testing.

Series	**Voxel ID**	**X_R (mm)**	**Z_R (mm)**	**Voxel Size (mm^3)**	**Percent Change: V1 Base**		
					mm^3	**X_R**	**Z_R**
1A,1B,5A,5B	V1	0.08	0.28	0.0023	0%	0%	0%
2A,2B,6A,6B	V2	0.08	0.39	0.0032	39%	0%	39%
3A,3B,7A,7B	V3	0.12	0.28	0.0034	50%	50%	0%
4A,4A,8A,8B	V4	0.12	0.39	0.0048	109%	50%	39%

Data Collection

The physical properties will be assessed with loss on ignition (LOI), tensile strength, scratch hardness, permeability, mass, and bonded density.

Loss on Ignition (LOI)

The procedure is performed with a sample size of three. A crucible mass is recorded, 25±5 grams of sand is added, and mass is recorded. Followed by a firing cycle at 1800°C for two hours, once cooled down to 68°F post fired weight is recorded. The weight loss of the sample is calculated to determine the loss on ignition of the sample. This is used to determine the amount of resin, catalyst, or moisture present in the sand. It is a standard test used by the foundry industry. American Foundry Society procedure AFS 5100-00-S

Tensile Strength

Industry accepted test method for the strength of the bonded sand under tension forces. This testing was completed using a Simpson Analytics pneumatic #42104 universal sand strength machine equipped with the tensile testing fixture. American Foundry Society procedure AFS 3301-08-S.

Scratch Hardness

Industry accepted test method for the measurement of exterior bonded sands resistance to damage during mold handling operations. American Foundry Society procedure AFS 3318-10-S.

Permeability

Permeability was measured by Dietert NO. 338-B electric Permmeter tester with the N0. 341-A attached for mold permeability. American Foundry Society procedure AFS 119-08-S.

Bonded Sand Density

The bonded sand density was calculated only for the rectangle 1” x 1.5” x 2” samples. The overall X,Y,Z measurement was taken using a fowler 6’ dial caliber. The mass was taken using a scale balance with accuracy of ±0.001 gram. Table 15 provides the test procedures along with how many data samples will be collected per procedure per trial.

Table 15. Test procedures and collection frequency

Test	Criteria per Trial
Loss on Ignition	Three samples from each orientation
Tensile Strength, Scratch Hardness, Permeability, and Mass.	Ten Samples per orientation for 30 total samples per trial
Part Density	Four rectangle samples per orientation for 12 total samples per trial

Data Analysis

For any printed samples the mean, median, standard deviation, and range will be calculated. Specifically, for the following tests: Loss on Ignition, Tensile Strength, Sample Mass, Printed Density, and Permeability.

The overall influence of the factors under investigation will be analyzed using Analysis of Variance (ANOVA) to determine the relationship of the key factors that impact the physical properties of the printed samples. The computer statistical analysis software SAS/STAT(R) will be used for the creation of the ANOVA.

CHAPTER 4

RESULTS AND DISCUSSION

Loss on Ignition

The test series with the smallest voxel, 1A, and 5A experienced the highest LOI as shown in Figure 20. As the voxel size increased, the LOI value was reduced. Series 4A and 8A dropped below the traditional targeted range for a Furan resin system.

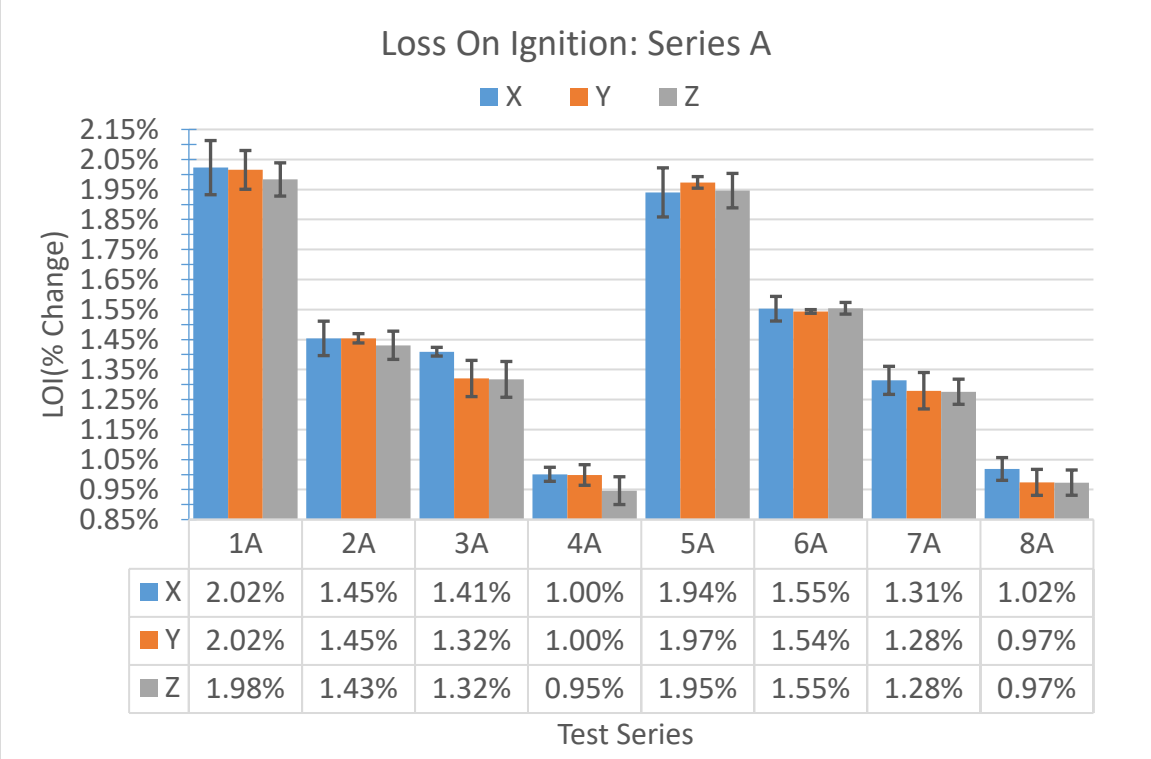

	1A	2A	3A	4A	5A	6A	7A	8A
X	2.02%	1.45%	1.41%	1.00%	1.94%	1.55%	1.31%	1.02%
Y	2.02%	1.45%	1.32%	1.00%	1.97%	1.54%	1.28%	0.97%
Z	1.98%	1.43%	1.32%	0.95%	1.95%	1.55%	1.28%	0.97%

Figure 20. LOI Results for eight trial Series A.

When the three samples per axis series were individually analyzed and grouped using Tukey ANOVA as shown in Table 16 the samples that were statistically different

were only 8% (4 out of 48). This demonstrates that the overall resin content printed between the axis' was the same and orientation did not impact the total resin content being printed.

Table 16. Individual ANOVA LOI and Axis same numeral means equivalent series.

One-Way ANOVA LOI, Axis								
Test Series A	Tukey Grouping			Test Parameters (GFN, X_R, Z_R)	Test Series B	Tukey Grouping		
	X	Y	Z			X	Y	Z
1A	I	I	I	57, 0.08, 0.28	1B	I	I,II	II
2A	I	I	I	57, 0.08, 0.39	2B	I	I	I
3A	I	I	I	57, 0.12, 0.28	3B	I	I,II	II
4A	I	I	I	57, 0.12, 0.39	4B	I	I	I
5A	I	I	I	70, 0.08, 0.28	5B	I	I	I
6A	I	I	I	70, 0.08, 0.39	6B	I	I	I
7A	I	I	I	70, 0.12, 0.28	7B	I	I	I
8A	I	I	I	70, 0.12, 0.39	8B	I	I	I

Since the axial statistical significance within the individual samples was determined to be the same, the nine data points were combined, and Tukey ANOVA using LOI and test series was calculated for each series as shown in Table 17. For series A 75% of the samples were statistically the same for the same machine parameters. For series B only 25% of the samples were statistically the same for the same machine parameters. There was no observed trend based upon the sand type and the measured resin content. Series 1B contained a much lower resin content than compared to 1A, 5A, and 5B.

Table 17. ANOVA by series LOI Comparison left is Series A, right is Series B.

Series A				
Means with the same numeral are not significantly different.				
Tukey	Grouping	Mean	N	series
	I	2.01%	9	1A
	I	1.95%	9	5A
	II	1.55%	9	6A
	III	1.45%	9	2A
	IV	1.35%	9	3A
	IV	1.29%	9	7A
	V	0.99%	9	8A
	V	0.98%	9	4A

Series B				
Means with the same numeral are not significantly different.				
Tukey	Grouping	Mean	N	series
	I	1.96%	9	5B
	II	1.78%	9	1B
	III	1.50%	9	6B
	IV	1.41%	9	2B
	V	1.31%	9	7B
	VI	1.23%	9	3B
	VII	0.97%	9	4B
	VII	0.91%	9	8B

Tensile Strength Results

Series 1A-4A, 1B-4B comprises the trials with the 57 GFN sand and Series 5A-8A, 5B-8B is the 70 GFN sand as shown in Figure 21. When examined at the upper and lower limits of resin content, both sands tensile strengths were within one standard deviation of the comparative sample. The low standard deviation demonstrates the repeatability of the printing process. However, when examining the middle series, there is a linear strength loss for the 57 GFN sand whereas the 70 GFN sand experiences a plateauing effect. The finer grain distribution retains a higher tensile strength with less resin content on the sand as confirmed by the LOI testing. When the 70 GFN drops below 1% resin threshold, the tensile strength matches that of the 57 GFN sand.

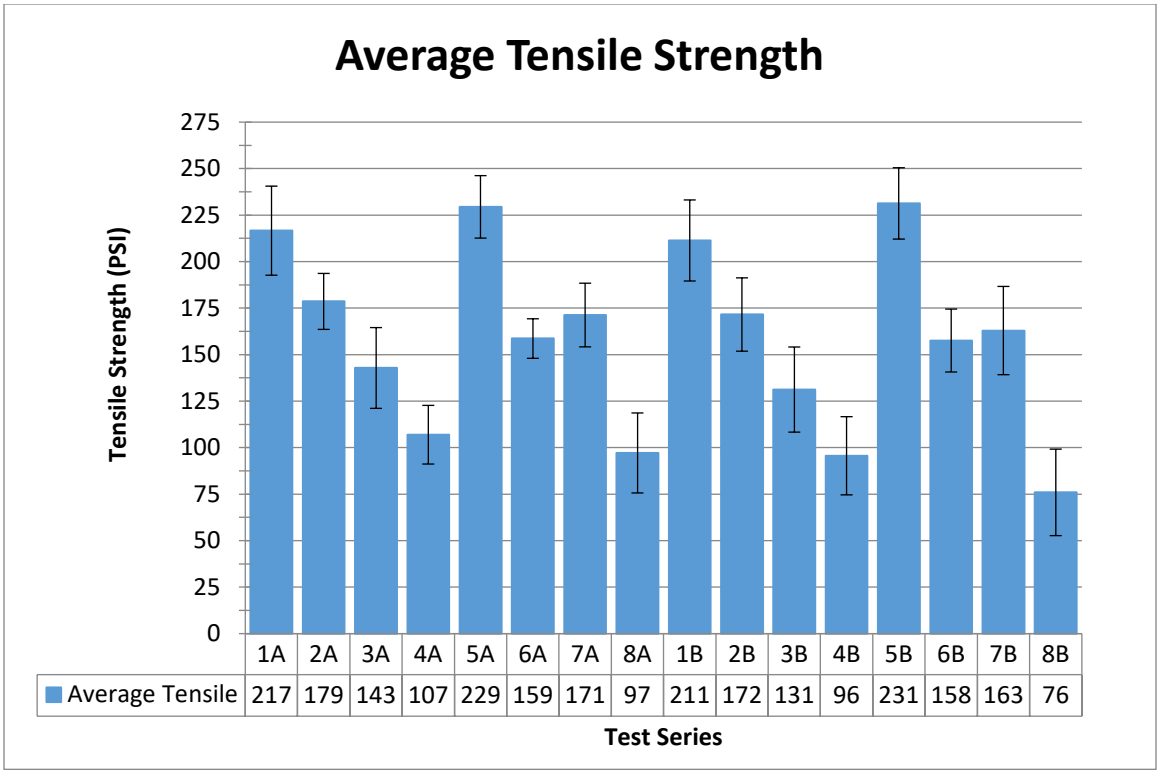

Figure 21 Tensile strength results for Series A and B dog bone samples.
Series 1A-4A and 1B-4B are the 57 GFN sand samples.
Series 5A-8A and 5B-8B are the 70 GFN sand samples.

The examination of the individual series for axial strength difference was performed using ANOVA with Tukey grouping, 14 out of the 16 samples reported a statistical difference in the Z-Axis tensile strength compared X and Y axis. The results of the ANOVA are shown in Table 18. Additionally, at the maximum resin content of 2%, 5A and 5B reported no statistical difference in the orthogonal strengths.

Table 18. Individual ANOVA Tensile and Axis.

One-Way ANOVA Tensile, Axis Note means with the same numeral are not significantly different.								
Test Series A	Tukey Grouping			Test Parameters (GFN, X_R, Z_R)	Test Series B	Tukey Grouping		
	X	Y	Z			X	Y	Z
1A	I	I	II	57, 0.08, 0.28	1B	I	II	II
2A	I	I	II	57, 0.08, 0.39	2B	I	I	II
3A	I	I	II	57, 0.12, 0.28	3B	I	I	II
4A	I	I	II	57, 0.12, 0.39	4B	I	I	II
5A	I	I	I	70, 0.08, 0.28	5B	I	I	I
6A	I	I	II	70, 0.08, 0.39	6B	I	I	II
7A	I	I	II	70, 0.12, 0.28	7B	I	I	II
8A	I	I	II	70, 0.12, 0.39	8B	I	I	II

The interaction effects of the sand type, X_R, and Z_R on tensile strength were examined using a three-way ANOVA in Table 19. The only interaction that was statistically significant was the combination of sand type and Z_R (<0.0001 p-value). The alpha level was the standard 0.05 for all ANOVA testing in this investigation.

Table 19. Three-way ANOVA Results Series A: Sand, X_R, Z_R, and Tensile

Dependent Variable: tensile					
Source	DF	Sum of Squares	Mean Square	F Value	Pr > F
Model	7	465337.37	66476.7671	199.16	<.0001
Error	232	77439.455	333.7908		
Corrected Total	239	542776.825			
R-Square	Coeff Var	Root MSE	tensile Mean		
0.857327	11.2295	18.26994	162.6954		
Source	DF	Type I SS	Mean Square	F Value	Pr > F
sand	1	493.3534	493.3534	1.48	0.225
xres	1	263668.475	263668.475	789.92	<.0001
sand*xres	1	2503.25	2503.25	7.5	0.007
zres	1	179640.288	179640.288	538.18	<.0001
sand*zres	1	18912.626	18912.626	56.66	<.0001
xres*zres	1	5.251	5.251	0.02	0.9
sand*xres*zres	1	114.126	114.126	0.34	0.559

ANOVA Treatment examination

To better understand the interaction effects the series was further analyzed by performing a treatment analysis using one-way ANOVA of treatment and tensile strength as shown in Table 20. The treatment value was coded such that series 1A is to 1, 2A is to 2, etc. This confirmed statistical significance between the samples (p-value <0.0001).

Table 20. ANOVA Treatment Analysis for Series A.

Dependent Variable: tensile					
Source	DF	Sum of Squares	Mean Square	F Value	Pr > F
Model	7	465337.37	66476.7671	199.16	<.0001
Error	232	77439.455	333.7908		
Corrected Total	239	542776.825			
R-Square	Coeff Var	Root MSE	tensile Mean		
0.857327	11.22954	18.26994	162.6954		
Source	DF	Type I SS	Mean Square	F Value	Pr > F
treatment	7	465337.37	66476.7671	199.16	<.0001
Source	DF	Type III SS	Mean Square	F Value	Pr > F
treatment	7	465337.37	66476.7671	199.16	<.0001

The treatment analysis showed that series 1A and 5A were statistical the same. Series 2A and 7A were the same. 7A overlapped with series 6A. Series 3A was unique. Series 4A and 8A were statistical the same. When the test parameters are compared, the upper and lower voxel sizes match between the two sand types. Only in the middle voxel sizes do the tensile strengths begin to overlap. Table 21 provides a summary of the treatment tukey grouping for tensile strength.

Table 21. Treatment Tukey Grouping for Tensile Strength.

Means with the same letter are not significantly different.					
Tukey Grouping		Mean	N	treatment	Test Parameters (GFN, XR, ZR)
	I	229.443	30	5	70, 0.08, 0.28
	I	216.66	30	1	57, 0.08, 0.28
	II	178.613	30	2	57, 0.08, 0.39
III	II	171.287	30	7	70, 0.12, 0.28
III		158.647	30	6	70, 0.08, 0.39
	IV	142.827	30	3	57, 0.12, 0.28
	V	106.947	30	4	57, 0.12, 0.39
	V	97.14	30	8	70, 0.12, 0.39

Axial Tensile Comparison

With the ANOVA analysis confirming that X and Y tensile samples were not different, an average of the X and Y axis was computed. This composite XY average was used to calculate the percent difference between average axial strength for each orientation. Figure 22 shows there was no apparent pattern for the X and Y strengths, the values randomly switched from positive to negative. However, there was a trend with the Z-axis that ANOVA analysis confirmed was statistically different from X and Y. As the voxel size increases the strength reduction along the Z increases greatly. The 70 GFN sand experienced a much greater strength loss in the Z-axis compared to the 57 GFN sand. Additionally, the Z strength loss was much greater when the resin was at 1% or when the voxel size was V4. This demonstrates based upon the furan resin system used in this investigation follows the traditional foundry rules of dropping below 1% resin content results in physical properties dropping below the desired values.

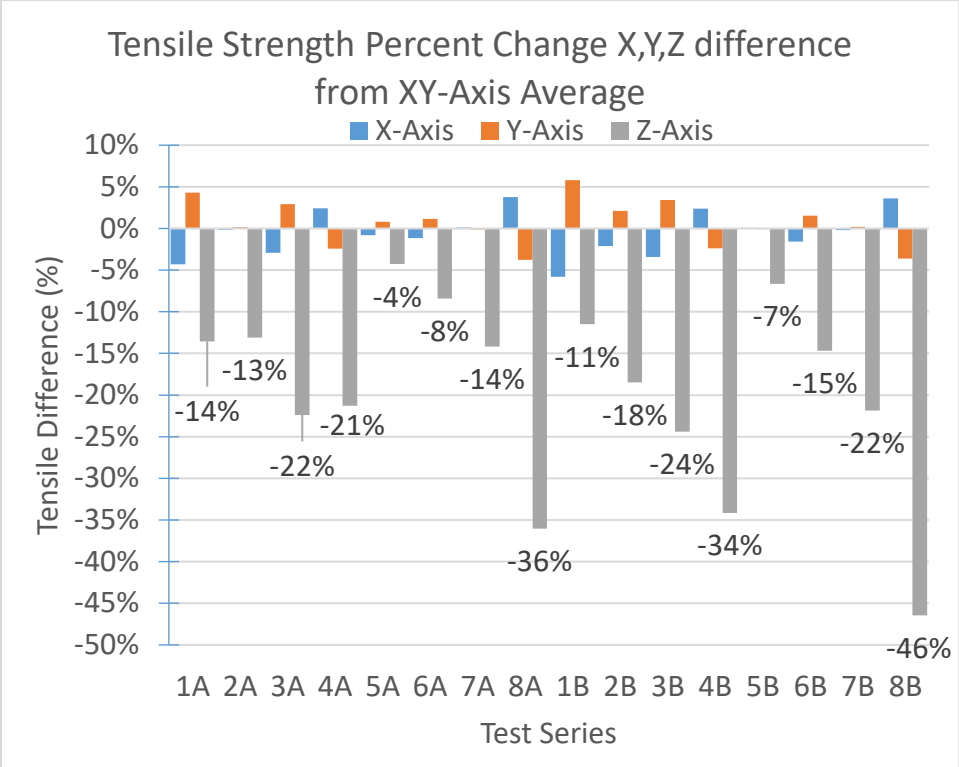

Figure 22. Compared Tensile strength to XY average percent change from average for X, Y, and Z axial Tensile strength.

Mass Results

The 57 GFN sand produced samples with a larger mass than the 70 GFN sand as shown in Figure 23. The LOI ANOVA testing confirmed samples contained equal amounts of resin present on the sand series. Due to the complex curves upon the tensile specimen's, part volume was unable to be calculated to determine a printed tensile specimen density.

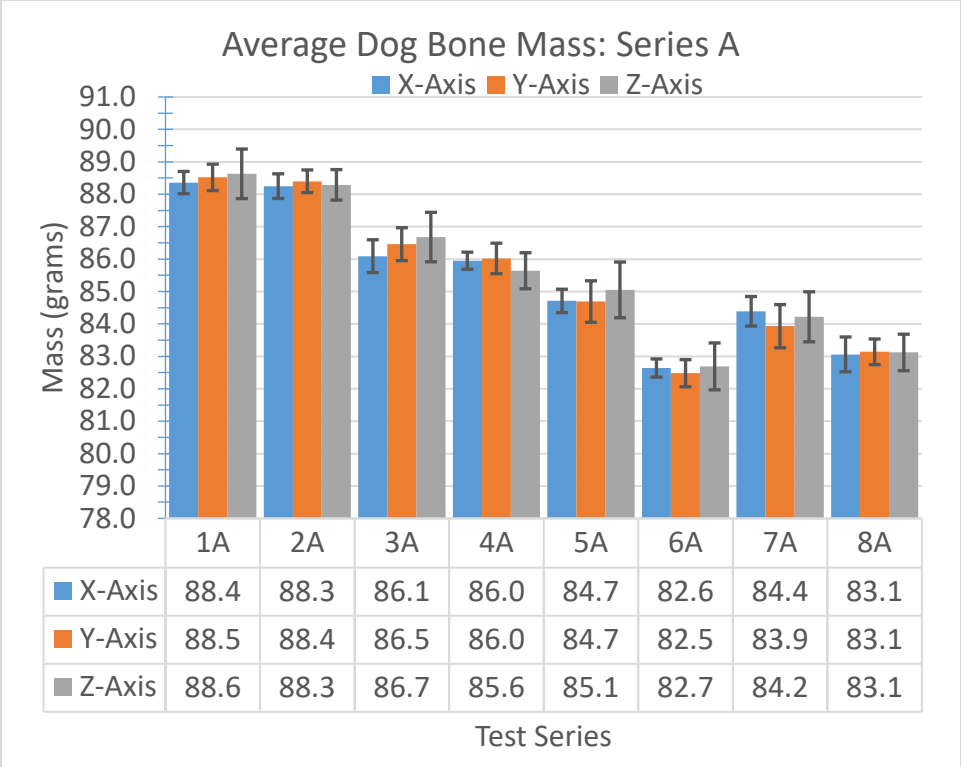

	1A	2A	3A	4A	5A	6A	7A	8A
X-Axis	88.4	88.3	86.1	86.0	84.7	82.6	84.4	83.1
Y-Axis	88.5	88.4	86.5	86.0	84.7	82.5	83.9	83.1
Z-Axis	88.6	88.3	86.7	85.6	85.1	82.7	84.2	83.1

Figure 23. Series A mass per axis of samples.

The mass of the individual series was analyzed to see if printing orientation had any influence on the dog bone mass. The Tukey ANOVA Table 22 confirmed there was no axial mass difference between the printed samples.

Table 22. Individual series one-way ANOVA mass specimen mass.

Single Series One-Way ANOVA Mass, Axis Note means with the same numeral are not significantly different.				
Test Series	Tukey Grouping			Test Parameters (GFN, X_R, Z_R)
	X	Y	Z	
1A	I	I	I	57, 0.08, 0.28
2A	I	I	I	57, 0.08, 0.39
3A	I	I	I	57, 0.12, 0.28
4A	I	I	I	57, 0.12, 0.39
5A	I	I	I	70, 0.08, 0.28
6A	I	I	I	70, 0.08, 0.39
7A	I	I	I	70, 0.12, 0.28
8A	I	I	I	70, 0.12, 0.39

The interaction effects of sand type, XR, ZR, on the dog mass was analyzed using a Three-way ANOVA Table 23. The combination of sand*xres, sand*zres, and sand*xres*zres was found to be statistically significant, (p-value of <0.0001).

Table 23. Three-way ANOVA sand, X_R, Z_R, and mass

Dependent Variable: mass					
Source	DF	Sum of Squares	Mean Square	F Value	Pr > F
Model	7	1026.692625	146.670375	490.65	<.0001
Error	232	69.352333	0.298932		
Corrected Total	239	1096.044958			
R-Square	Coeff Var	Root MSE	mass Mean		
0.936725	0.639654	0.546747	85.47542		
Source	DF	Type I SS	Mean Square	F Value	Pr > F
Sand	1	776.520375	776.520375	2597.64	<.0001
Xres	1	81.783375	81.783375	273.58	<.0001
sand*xres	1	72.7100417	72.7100417	243.23	<.0001
Zres	1	60.5010417	60.5010417	202.39	<.0001
sand*zres	1	24.5120417	24.5120417	82	<.0001
xres*zres	1	2.340375	2.340375	7.83	0.0056
sand*xres*zres	1	8.325375	8.325375	27.85	<.0001

To better understand the interaction effects the series was further analyzed by performing a treatment analysis using one-way ANOVA of treatment and tensile strength Table 24. The treatment value was coded such that series 1A is to 1, 2A is to 2, etc. This confirmed statistical significance between the samples,(p-value of <0.0001).

Table 24. ANOVA results for treatment mass analysis

Dependent Variable: mass					
Source	DF	Sum of Squares	Mean Square	F Value	Pr > F
Model	7	1026.692625	146.670375	490.65	<.0001
Error	232	69.352333	0.298932		
Corrected Total	239	1096.044958			
R-Square	Coeff Var	Root MSE	mass Mean		
0.936725	0.6397	0.546747	85.47542		
Source	DF	Type I SS	Mean Square	F Value	Pr > F
treatment	7	1026.692625	146.670375	490.65	<.0001
Source	DF	Type III SS	Mean Square	F Value	Pr > F
treatment	7	1026.692625	146.670375	490.65	<.0001

The treatment analysis demonstrated for the 57 GFN samples that Series 1A and 2A were the same regardless of the change in the Z_R as shown in Table 25. Whereas the 70 GFN experienced the greatest mass change from the Z_R Series 6A and 8A at 0.39 mm were much lighter than the 0.28mm Z_R samples.

Table 25. Tukey Grouping for Treatment ANOVA analysis

Means with the same letter are not significantly different.				
Tukey Grouping	Mean	N	treatment	Test Parameters (GFN, XR, ZR)
I	88.5033	30	1	57, 0.08, 0.28
I	88.3133	30	2	57, 0.08, 0.39
II	86.41	30	3	57, 0.12, 0.28
III	85.87	30	4	57, 0.12, 0.39
IV	84.8167	30	5	70, 0.08, 0.28
V	84.18	30	7	70, 0.12, 0.28
VI	83.1067	30	8	70, 0.12, 0.39
VII	82.6033	30	6	70, 0.08, 0.39

Spreading Characteristics

The coarser distribution of 57 GFN free flowed evenly during recoating; note the uniform wave front in the left image of Figure 24. The 70 GFN would exit the recoater in clumps that would break apart. The uneven wave front is where one of the clumps would break apart and spread in front of the recoater right image of Figure 24. If a smaller gap opening were used with the 70 GFN sand, the recoater would plug and result in layers with improper spreading. Too large of a gap opening uses excess during recoating and additionally can result in pushing of the part geometry during recoating. This observed large difference in spreading characteristics is the likely cause for the large difference between the printed dog bone mass.

Figure 24. Image capture from video of sand spreading during recoating cycle of during printing of sand trials. Left image 530 spreading and right image is the 510 spreading.

Density Results

The standard deviation of the printed sample was too great for ANOVA analysis as shown in Figure 25. However, the average printed density across all samples was 1.283 g/cm^3. Visually inspections show that both sand types printed very close to the total average. Additionally, no axial printing difference can be observed.

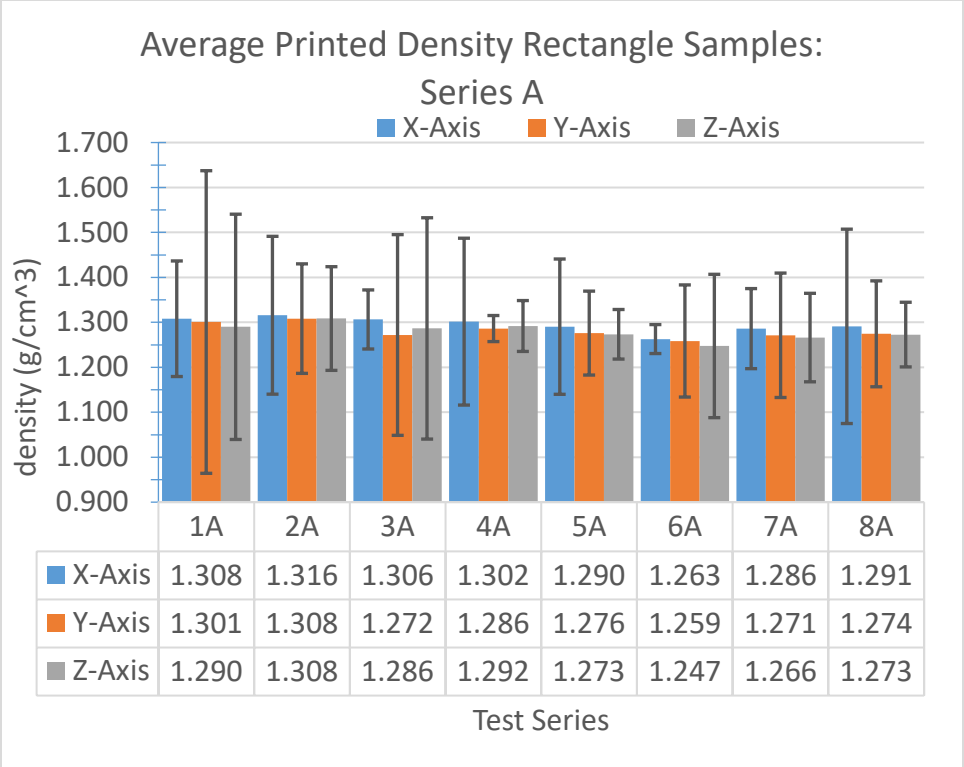

Figure 25. Four sample average of printed rectangle's for density analysis

Overall Results

Total Average Scratch Hardness

The surface sand hardness mirrors the results observed by the tensile strength analysis. The plateau effect for the middle 70 GFN samples is also present in the scratch hardness results as shown in Figure 26. As the resin level dropped below 1%, the variability within the surface hardness increased.

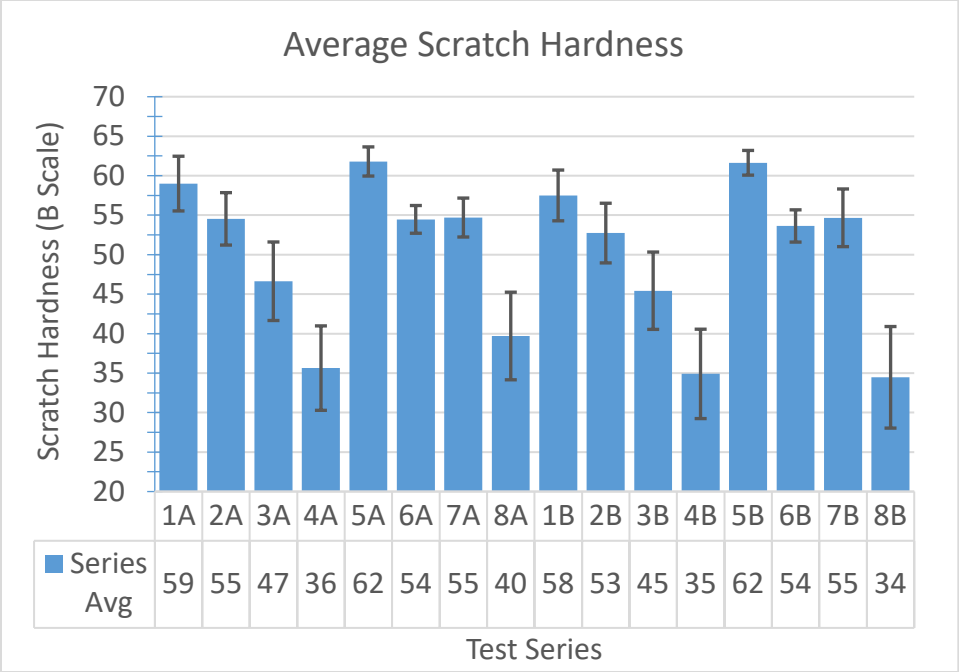

Figure 26. Average scratch hardness for all test series.

Axial Scratch Hardness

The XYZ axial scratch hardness is shown in Figure 27. The variability increases along the Z_R as the voxel size increases and the resin content is reduced. When the means are examined for the individual series, the trend is observed that the Z_R samples are statistically significantly lower than the X and Y axis as shown in Table 26. Roughly 61% of the samples experienced lower surface hardness in the Z-axis compared to X and Y axis.

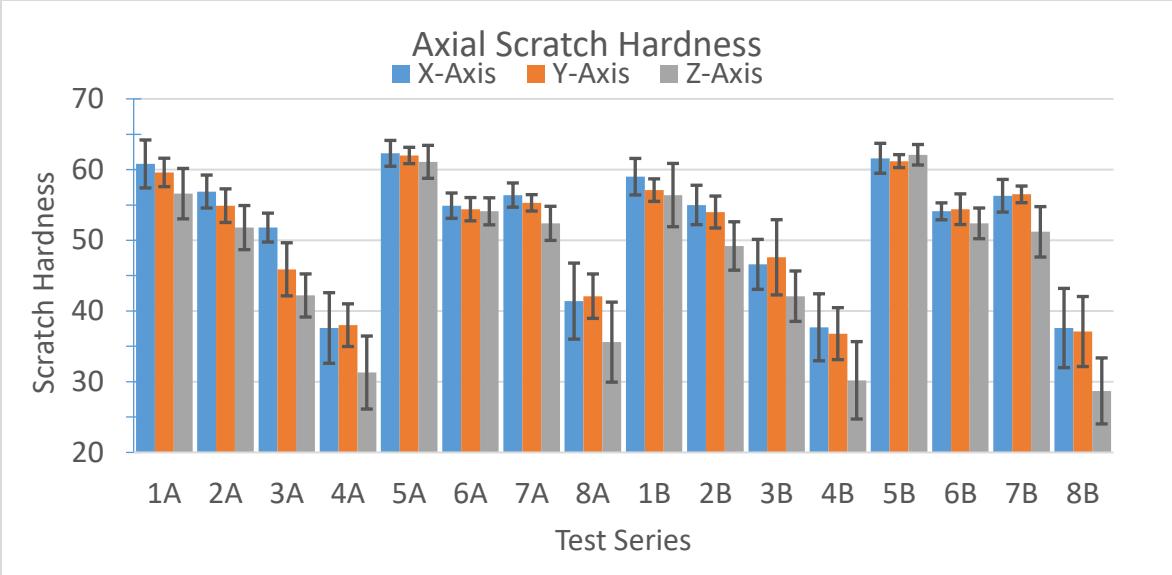

Figure 27. Scratch Hardness Comparison of Orthogonal Axis.

Table 26. Individual Series ANOVA Scratch Hardness Series 1A and 1B Comparison.
One-Way ANOVA Scratch Hardness, Axis
Note means with the same numeral are not significantly different.

Test Series	Tukey Grouping			Test Parameters (GFN, X_R, Z_R)	Test Series	Tukey Grouping		
	X	Y	Z			X	Y	Z
1A	I	I,II	II	57, 0.08, 0.28	1B	I	I	I
2A	I	I	II	57, 0.08, 0.39	2B	I	I	II
3A	I	II	III	57, 0.12, 0.28	3B	I	I,II	II
4A	I	I	II	57, 0.12, 0.39	4B	I	I	II
5A	I	I	I	70, 0.08, 0.28	5B	I	I	I
6A	I	I	I	70, 0.08, 0.39	6B	I	I	I
7A	I	I	II	70, 0.12, 0.28	7B	I	I	II
8A	I	I	II	70, 0.12, 0.39	8B	I	I	II

The individual axial tensile strength ANOVA determined that the X and Y series were statistical the same, this allowed the ability to combine both dataset into a single average. The individual tensile XY datasets were combined to make a composite XY

average, which was used to calculate the percent change of the three individual axis as shown in Figure 28. The Z-axis experiences a greater loss of scratch hardness than compared to the X and Y values.

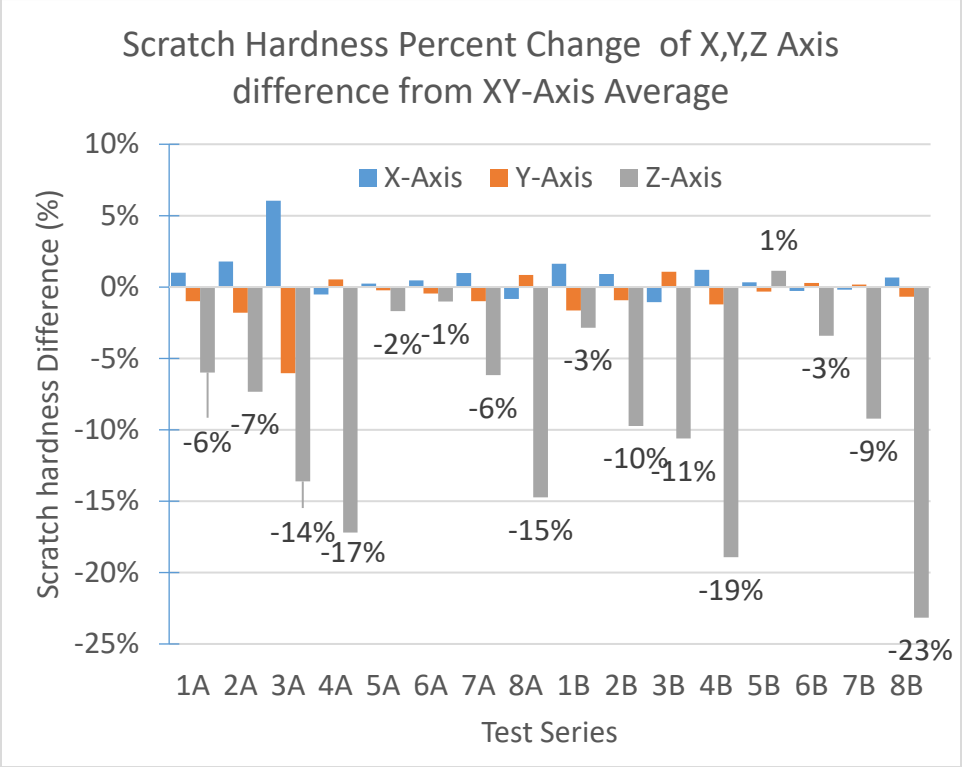

Figure 28. Overall Scratch Hardness comparisons to axial percent change.

Permeability

The permeability difference between the two sand distributions is shown in Figure 29. The average permeability of the 57 GFN sand was 442, and the 70 GFN sand was 260. The 70 GFN sand did experience an increase in permeability in three out of the

four samples printed at 0.39 mm Z_R (6A, 6B, 8B). This was outside the standard deviation.

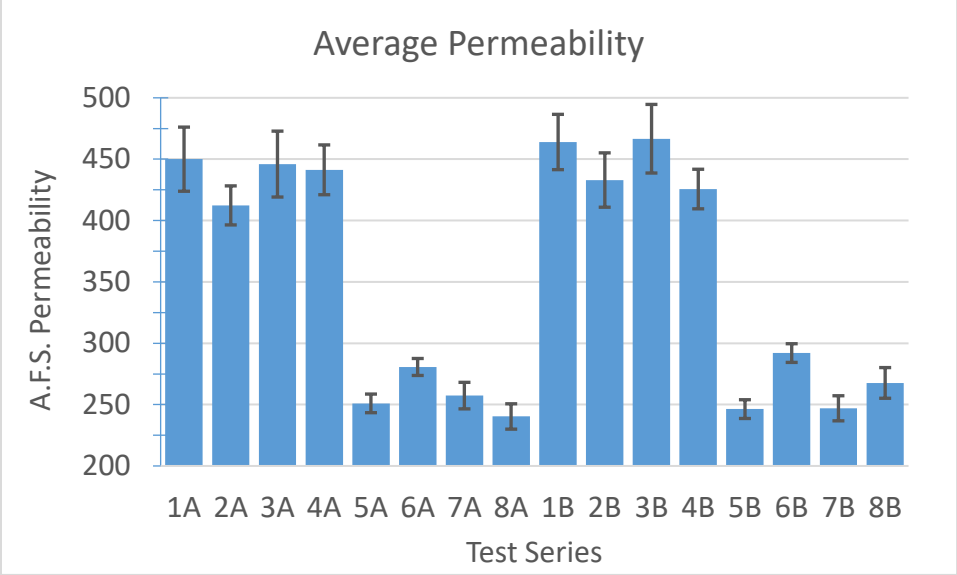

Figure 29. Average permeability results for all test series.

Average Tensile and LOI Comparison

When the average tensile strength of all series was plotted with the LOI value on the secondary axis as shown in Figure 30, the strength plateau of the 70 GFN sand was more apparent. Replicate series of 7A and 7B series exhibited tensile strengths higher than the 6A and 6B series with having a lower LOI value by 0.01%. When comparing the 57 GFN to 70 GFN at the resin level of 1.2%-1.3%. The 3A and 3B series 57 GFN were 143 and 131 PSI whereas the equivalent 70 GFN series 7A and 7B were 171 and 163 PSI. This demonstrates given the same machine settings the 70 GFN sand retained a higher strength with a lower amount of resin present on the sand.

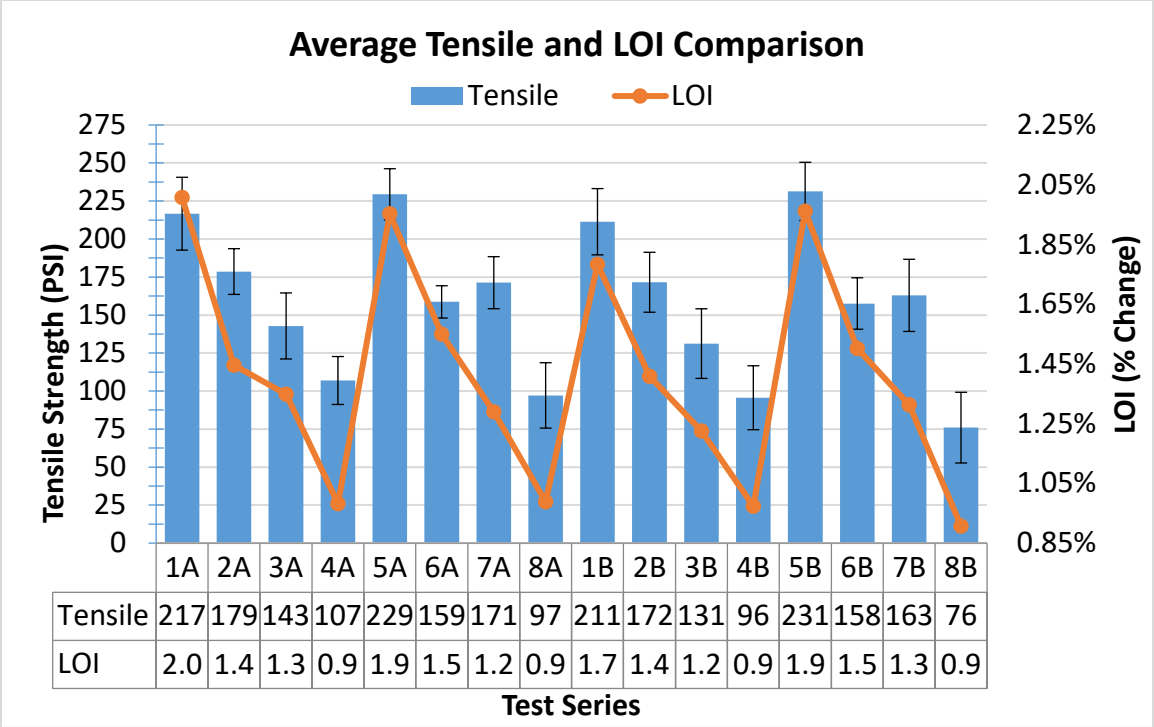

	1A	2A	3A	4A	5A	6A	7A	8A	1B	2B	3B	4B	5B	6B	7B	8B
Tensile	217	179	143	107	229	159	171	97	211	172	131	96	231	158	163	76
LOI	2.0	1.4	1.3	0.9	1.9	1.5	1.2	0.9	1.7	1.4	1.2	0.9	1.9	1.5	1.3	0.9

Figure 30. Full series comparison of tensile with secondary axis overlay of LOI results.

Average Tensile and Voxel Aspect Changes

Recall that Table 14 provides the machine parameters along with the corresponding voxel size, test series, and associated $X_{R,}$ and Z_{R} percent volume changes from voxel size V1. The X and Z axis volume changes are graphed on the secondary axis of the tensile strength chart as shown in Figure 31. This comparison more readily highlights how both machine settings for voxel size V2 and V3 produce nearly identical tensile strengths. The V3 voxel size is 8% larger than the V2 voxel size. When the voxel size is increased to V4 0.0048 $mm^{3,}$ there is a substantial observed strength reduction.

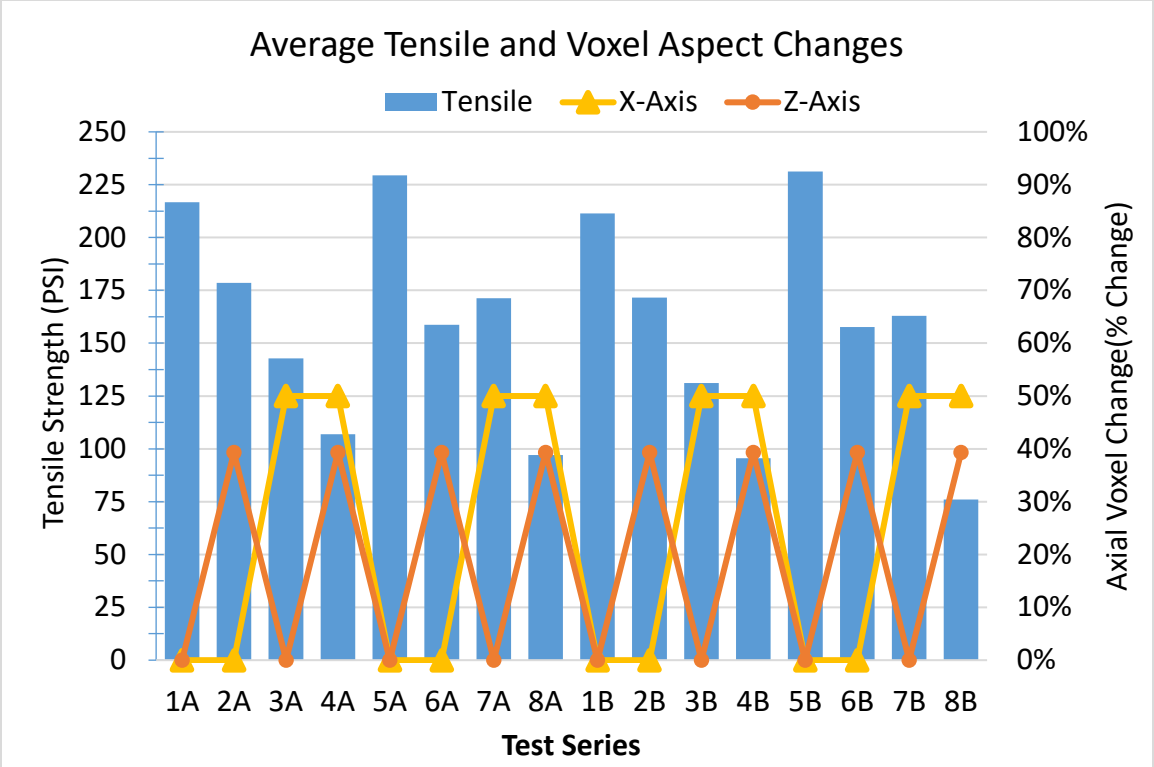

Figure 31. Series average tensile strength with secondary axis axial voxel percent change.

Discussion

The stark spreading difference between the two sand types is likely the attributing factor for the observed mass difference between the printed dog bones. The finer grain 70 GFN silica sand produced an overall lighter dog bone sample than the coarse grain 57 GFN silica sand. The 70 GFN has peak retention on the 100 mesh and doubles the retention of the 140 and 200 mesh comparative the 57 GFN sand. This large increase of smaller grains with an equal weight percent of liquid acid catalyst likely contributes to an increased grain to grain acid catalyst capillary force across the small

screen meshes in the 70 GFN as noted by the research conducted by Harireche et al., (2013). and Gras, Delenne, & El Youssoufi, (2013).

The ANOVA research confirmed that as X_R, Z_R, and sand type did impact the printed sand mass. The X_R and Z_R should influence the dog mass since the droplet size is fixed by the machine operator and any voxel size changes would result in an individual droplet contributing less mass per voxel. The overall resin content present on the sand test series for a specified machine parameter was within ±0.03% if the outlier of the 1B test series LOI value of 1.78% is removed.

The large variation associated with the printed density samples is attributed to the small mass and size of the samples. The density samples weighed between 16 to 18 grams depending on the sand type used. Additionally, only four samples per orientation were able to be arranged into the build envelopment while maintaining the lowest build height possible. However, even with the variation present, it was still observed that regardless of the sand type utilized both series printed, with roughly the same density of 1.3 g/cm^3 or 81 lbs/ft^3. This observed printed sand density mirrors the silica results from Coniglio et al. (2018) and Nyembwe et al. (2016) research findings for 3D printed silica sand. The observed density reduction compared to traditional produced cores appears to inherit to the 3D sand printing when a recoater strike off device is utilized for compaction. The usage of a compaction roller might allow an increase in printed sand density.

The tensile results provided the greatest insight into the impact of screen distribution on performance characteristics of the sands tested. Both aggregates performed the same at the upper limit of the tested resin content at 1.9-2.0% (X_R 0.08, Z_R 0.28) with tensile strengths of 211-231 PSI. The lower limit of the tested resin content of 0.9% both aggregate performed the same with a tensile strength of 76-107 PSI. It was only in the middle resin contents ranging from 1.2-1.5% (X_R 0.12, Z_R 0.28 & X_R 0.08, Z_R 0.39) that there was an observed difference between the sand aggregates. The 57 GFN exhibited a linear strength reduction as the voxel size increased and the resin content present decreased. The 70 GFN experienced a plateau of the tensile strength. The 7A/B samples maintained a tensile of 163-171 PSI with roughly 0.2% lower resin content present on the sand compared to the 6A/B samples that had 1.5% (X_R 0.08, Z_R 0.39) resin content and a tensile strength of 158 and 159. The increased tensile strength of the 70 GFN at V3 voxel size is likely attributed to the greater percentage of binder bridges present within a finer grain distribution as Nagai et al., (2016) demonstrated that a particular screen distribution can retain a greater volume of resin present at the grain to grain contact points. It is possible that the combination of the resin droplet to V3 voxel size is the optimal resin volume to contact points per volume. Further examination with SEM, CT, or optical microscopes would be needed to confirm.

The comparison of voxel ID's V2 X_R 0.08 mm Z_R 0.39 mm with V3 X_R 0.12 mm Z_R 0.28 mm showed that both machine parameters produce similar tensile strengths. The largest benefit to printing at Z_R 0.39 mm would be reduction of printing time. In the

case of the tensile specimens, the 0.28 mm layer thickness requires 272 layers to complete, whereas the 0.39mm layer thickness only requires 195 layers to complete. Such a machine parameter change can reduce the total build time for a job by 28%. Note with the increased layer thickness an operator would have to balance increased surface roughness due to the larger layer thickness.

The axial performance between the two screen distributions highlighted an additional area that the distribution impacted. The ANOVA analysis confirmed that both aggregates experienced a reduction in the Z-axis strength compared to the X and Y-Axis. This reduction was observed in both the tensile strength and the scratch hardness. The 70 GFN sand experienced a higher reduction in the Z-axis strength compared to the 57 GFN sand since the 70 GFN sand retains more contact points per volume this would agree with Nagai et al., examination of the shell sand contact points.

This Z-axial tensile strength difference is very minor (10 to 18%) when the resin level is above 1.4% (X_R 0.08, Z_R 0.39), but as the resin level drops the disparity in the Z-axis tensile strength increases. The 70 GFN sand experienced a much larger Z tensile drop at 36% to 46% than compared to the 57 GFN Z tensile drop of 22% to 34%. This axial strength reduction should be an area of concern for future sand printers that could dynamically adjust the resin content level within localized areas within the build box.

The scratch hardness also observed that there was a performance difference between the X, Y, and the Z surfaces. The Z hardness was in the YZ and XZ planes while

the X and Y hardness samples were both in XY plane. The combination of the tensile data (internal core performance) and the scratch hardness (exterior sand performance) demonstrates this issue is only along the Z-axis. The Z-axis at 0.39 mm is 3.25 times larger than the widest X_R parameter of 0.12mm and is 39% thicker than the 0.28 mm Z_R parameter. Since the LOI at the voxel size V4 drops below 1% resin content this voxel size is likely too large for the resin droplet being placed within it. If an operator wishes to print a larger sand layer thickness, the X_R must be reduced to bring the resin content back above 1% or a larger droplet mass could use in lieu of an X_R adjustment.

This investigation supported the traditional foundry resin usage levels for a Furan binder system that when the resin content drops below 1% resin (X_R 0.12, Z_R 0.39), the performance of the resin system and the sand aggregate is negatively impacted, with proper machine settings a larger layer thickness could be printed without the observed Z-axis performance degradation.

CHAPTER 5

CONCLUSION AND RECOMMENDATIONS

Conclusion

While 3DPS proves to disrupt the design rules for castings the traditional foundry guidelines for a Furan resin system require that at least 1% resin be present for sufficiently rigid molds or cores. This investigation demonstrated that if the resin level is below 1% there becomes an issue of anisotropic strength properties specifically along the Z-axis. If the resin level within the bonded sand is above 1%, the anisotropic properties are of the Z-axis is reduced to an acceptable level.

The influence of screen distribution on the performance properties of 3DPS at the upper level of 2% (X_R 0.08, ZR 0.28) resin content showed no difference between the 57 GFN and 70 GFN tested sands. Similarly, when the resin level dropped below 1% (X_R 0.12, Z_R 0.39) resin, both screen distributions experienced the previously discussed anisotropic properties.

Only in the middle values of 1.3% (X_R 0.12, Z_R 0.28) to 1.5% (X_R 0.08, Z_R 0.39) resin was there a statistically different performance between the two screens. The 57 GFN experienced a linear strength reduction as resin content was reduced. The 70 GFN experienced a strength plateau where the lower resin content of 1.3% (X_R 0.12, Z_R 0.28) resin retained a similar strength level to the 1.5% (X_R 0.08, Z_R 0.39) resin series. This

demonstrated that for a given resin content on the printed sand the 70 GFN performed better when above 1% (X_R 0.12, Z_R 0.39) resin. This research demonstrated there is an optimal level for tensile strength, LOI, and voxel size for a sand distribution.

Recommendations for Future Studies

1. Selection of a test specimen that allows for the measurement of part volume such that strength data can be compared with density data. Due to the size limitations in the Z-axis of 150 mm the traditional 25.6 mm x 25.6 mm x 203.2 mm transverse bar could not be used. Even though the dog bone is an industry accepted test specimen for tensile strength, the curved geometric features of the dog bone make determining the part volume a problematic endeavor. The rectangle density samples utilized in this investigation proved to be insufficient in size to provide reliable data.
2. The observed axial strength difference at lower resin content demonstrated that the ability to examine the resin volume and frequency of contact points would provide greater insight. This could be done with the use of SEM, CT scanning, or high powered optical microscope.
3. The inclusion of different screen distributions, sand types, and sand suppliers beyond the investigated round grain three screen silica sand utilized in this investigation, would provide a greater understanding of how the printing performance of a 3D sand printer is affect by the sand type utilized.

REFERENCES

AFS Mold and Core Test Handbook (Vol. 4th Edition). (2015). Schaumburg, IL: American Foundry Society.

Booth, B.H., & Sanders, C.A., (1954). Another Look at Sand Grain Distribution. *Transactions of the American Foundry Society, 62*, 499-506.

Celauro, C., Ziccarelli, M., Parla, G., & Valore, C. (2014). An automated procedure for computing the packing properties of dense and locked sands by image analysis of thin sections. *Granular Matter, 16*(6), 867-880.

Coniglio, N., Sivarupan, T., & Mansori, M. (2018). Investigation of process parameter effect on anisotropic properties of 3D printed sand molds. *The International Journal of Advanced Manufacturing Technology*, 94(5), 2175-2185.

Djebbar, T. , & Donaldson, E., (2012). *Petrophysics theory and practice of measuring reservoir rock and fluid transport properties* (3rd ed.). Boston: Gulf Professional Pub./Elsevier.

ExOne, (2012). *History ExOne*. Retrieved April 12, 2018 from ExOne website:http://www.exone.com/About-ExOne/History

Fairmount Santrol, Wedron Silica. (2014). Wedron Silica Sand. Retrieved from Fairmount Santrol website: http://fairmountsantrol.com/wp-content/uploads/2014/09/FM-0558_Wedron_SilicaSand_Sheet.pdf

Fisher, R. (1970). *Statistical methods for research workers.*(14th ed., revised and enlarged. ed.). Edinburgh, SCT: Oliver and Boyd.

Gras, J., Delenne, J., & El Youssoufi, M. (2013). Study of capillary interaction between two grains: A new experimental device with suction control. *Granular Matter, 15*(1), 49-56.

HA International LLC., Technical Data Sheet. (2004) *TSA & BSA Acid Catalyst*. Retrieved from HA International website: http://www.ha-international.com/tds/345283.pdf

HA International LLC., Technical Data Sheet. (2014) *Enviroset 3D Jet Resin*. Retrieved from HA International website: http://www.ha-international.com/tds/371381.pdf

Hackney, P. M., & Wooldridge, R. (2017). Characterisation of direct 3D sand printing process for the production of sand cast mould tools. *Rapid Prototyping Journal*, 23(1), 7-15.

Harireche, O., Faramarzi, A., & Alani, A. (2013). A toroidal approximation of capillary forces in polydisperse granular assemblies. *Granular Matter, 15*(5), 573-581.

Heine, R., & Seaton, T. (1958). Density of Sand Grain Fractions of the AFS Sieve Anaylis. *Transactions of the American Foundry Society, 86*, 40-45.

Nagai, S., Kannoi, A. , Ameku, H., Edane, K., Huang, Z., & Kurokawa, Y. (2016). In Relationship Between Sand-Grain Points of Contact in Shell Molds and Transverse Strength, Estimated Using X-Ray Computed Tomography. *Transactions of the American Foundry Society, 124*, 103-111.

Nelson, B., (1973). Density of Sand Grain Fractions of the AFS Sieve Anaylis. *Transactions of the American Foundry Society*, 94, 153-157.

Nyembwe, K., Mashila, M., Van Tonder, P., De Beer, D., & Gonya, E. (2016). Physical properties of sand parts produced using a Voxeljet VX1000 three-dimensional printer. *South African Journal of Industrial Engineering*, 27(3), 136-142.

Oda, M. (1972), Initial fabrics and their relations to mechanical properties of granular material, *Soils and Foundations (Jap. Soc. Soil Mech. Found. Engr.) 12*, 17.

Ott, L., & Longnecker, M. (2010) *An introduction to statistical methods and data analysis* Belmont, CA : Brooks/Cole Cengage Learning

Pedicini, L. J. (1958). Packing Characteristics of Typical Foundry Sands. *AFS Transactions*, *66*, 421.

Pinson, D., Zou, R.P, Yu, A.B., Zulli, P., & McCarthy, M. (1998). Coordination number of binary mixtures of spheres. *Journal of Physics D: Applied Physics, 31*(4), 457-462.

Sahoo, M. & Sahu, S. (2014). *Principles of Metal Casting.* New York City, NY: McGraw-Hill Education.

Sanders, C.A., & Doelamn, R., (1968). A Review of Sand Surface Area Relations. *Transactions of the American Foundrymen's Society*, *70*, 85-91.

Schleg, F. P. (2003). *Technology of Metalcasting*. Schaumburg, IL: American Foundry

Scott, W. D., Easterly, W. C., Lodge, P., & Blackburn, C. S. (2004). Foundryman's Guide to Sand Compaction. *Transactions of the American Foundry Society, 112*, 609-621.

Seaton, T. W. (1960). Density-Sand Grain Distribution Effect on Physical Properties. *AFS Transactions*, *68*, 40-45.

Smith, W.O., Foote, P.D., & Busang, P.F. (1929). Packing of homogeneous spheres. *Physics Review*, *34*(9), 1271-1274.

Snelling, D., Blount, H., Foram, C., Ramsburg, K., Wentzel, A., Williams, C., & Duschitz, A. (2013) *The effects of 3D Printed Molds on Metal Castings*, Solid Freedom Fabrication Symposium. Austin, TX.

Thiel, J., Ravi, S., & Bryant, N. (2017). Advancements in Materials for Three-Dimensional Printing of Molds and Cores. *International Journal of Metalcasting, 11*(1), 3-13

Thiel, J., Ziegler, M., Dziekonski, P., & Joyce, S. (2007). Investigation into the Technical Limitations of Silica Sand Due to Thermal Expansion. *Transactions of the American Foundry Society*, *115*, 383-400.

Thoury, M, Mille B., Séverin-Fabiani, T., Robbiola, M., Réfrégiers, M., Jarrige, J., & Bertrand, L. (2016). High spatial dynamics-photoluminescence imaging reveals the metallurgy of the earliest lost-wax cast object. *Nature Communications, 7*, 13356.

Voxeljet, 3D Printer VX200. (2016) VX200 The Compact entry into the world of 3D Printing. Retrieved from Voxeljet website: https://www.voxeljet.com/fileadmin/user_upload/PDFs/voxeljet_3d-printer_VX200_2016.pdf

Wiącek, & Molenda. (2014). Microstructure and micromechanics of polydisperse granular materials: Effect of the shape of particle size distribution. *Powder Technology,268*, 237-243.

Woods, K., & Ravi, S. (2015). Design considerations for 3-D-printed cores and molds: *Modern Casting, 105*(5), 24.

Woods, K., Richardson, M. & Trikha, S. (In Press). Premlinary Investigation and Method to Determine Resin Content for 3D Sand Printers. *Transactions of the American Foundry Society.*

APPENDIX A

DATA TABLES FOR EACH SERIES

Table A1. Collected data set for test series 1A and machine parameters.

	Print Order	Test	Sand
DOE Trial #	1	1A	530

X-Res	Z-Res
0.08	0.28

X-Axis				
Sample	Mass	Tensile	Scratch	Perm
1	88.7	245.4	62.0	400.0
2	88.2	224.8	64.0	420.0
3	88.0	219.4	60.0	440.0
4	88.6	215.4	65.0	420.0
5	88.3	211.6	61.0	440.0
6	88.6	197.2	55.0	440.0
7	88.9	198.0	63.0	440.0
8	87.8	224.4	62.0	460.0
9	88.4	204.2	55.0	460.0
10	88.1	231.2	61.0	440.0
Avg	88.36	217.16	60.8	436
σ	0.344	15.195	3.393	18.379

Z-Axis				
Sample	Mass	Tensile	Scratch	Perm
1	88.3	217.8	59	440
2	89.3	204	56	440
3	88.3	189.2	58	480
4	89	206	61	480
5	88.1	164.2	50	500
6	88.3	177.8	53	500
7	89.7	203.6	53	480
8	89.8	211.4	60	480
9	87.7	175.2	57	460
10	87.8	212.4	59	480
Avg	88.63	196.16	56.6	474
σ	0.765	18.331	3.565	21.187

LOI-X				
	Crucible	Before	After	%LOI
1	49.046	74.392	73.853	2.13%
2	37.816	62.627	62.140	1.96%
3	19.931	45.400	44.896	1.98%
%LOI	σ	0.09%	Avg	2.02%

LOI-Z				
	Crucible	Before	After	%LOI
1	34.732	59.720	59.234	1.94%
2	30.412	55.433	54.943	1.96%
3	32.808	57.529	57.023	2.05%
%LOI	σ	0.06%	Avg	1.98%

Y-Axis				
Sample	Mass	Tensile	Scratch	Perm
1	88.3	219.8	61	420
2	88.8	243.6	57	460
3	88.8	204	58	460
4	88.6	252.4	63	440
5	88.9	249.4	58	460
6	88.4	256	61	440
7	88.8	250.8	61	440
8	87.9	211.2	60	420
9	87.8	228	57	460
10	88.9	251.4	60.0	400.0
Avg	88.52	236.66	59.6	440
σ	0.408	19.217	2.011	21.082

X-Density Block				
Sample	Mass	X-Axis	Y-Axis	Z-Axis
1	18.715	1.547	1.043	0.545
2	18.234	1.542	1.039	0.532
3	18.706	1.545	1.038	0.543
4	18.276	1.542	1.038	0.529
Avg	18.483	1.544	1.040	0.537

LOI-Y				
	Crucible	Before	After	%LOI
1	33.707	57.261	56.802	1.95%
2	31.496	56.059	55.563	2.02%
3	36.534	60.454	59.957	2.08%
%LOI	σ	0.06%	Avg	2.02%

Y-Density Block				
Sample	Mass	X-Axis	Y-Axis	Z-Axis
1	18.714	1.038	1.542	0.546
2	18.526	1.04	1.538	0.533
3	18.199	1.04	1.541	0.536
4	18.284	1.045	1.536	0.544
Avg	18.431	1.041	1.539	0.540

Z-Density Block				
Sample	Mass	X-Axis	Y-Axis	Z-Axis
1	18.493	0.54	1.043	1.534
2	18.538	0.542	1.047	1.534
3	18.245	0.547	1.039	1.538
4	18.107	0.539	1.04	1.539
Avg	18.346	0.542	1.042	1.536

Table A2 Collected data set for test series 2A and machine parameters.

Print Order		Test	Sand
DOE Trial #	2	2A	530

X-Res	Z-Res
0.08	0.39

X-Axis				
Sample	Mass	Tensile	Scratch	Perm
1	87.8	179.0	58.0	420.0
2	88.3	181.6	59.0	400.0
3	88.5	165.8	57.0	400.0
4	88.5	194.4	59.0	400.0
5	88.2	182.2	53.0	400.0
6	88.3	185.4	56.0	410.0
7	87.6	192.4	58.0	420.0
8	87.9	204.0	60.0	400.0
9	88.8	185.0	54.0	390.0
10	88.6	194.8	55.0	400.0
Avg	88.25	186.46	56.9	404
Std Dev	0.381	10.557	2.331	9.661

Z-Axis				
Sample	Mass	Tensile	Scratch	Perm
1	88.4	166.2	51	420
2	88.2	154.6	53	420
3	88.8	165.2	51	440
4	88.8	177.4	52	420
5	88.7	164.6	56	420
6	88	165.2	54	420
7	88.1	145.2	46	460
8	88.6	160.8	50	420
9	88	168.8	56	420
10	87.3	155	49	420
Avg	88.29	162.3	51.8	426
Std Dev	0.470	8.912	3.120	13.499

LOI-X				
	Crucible	Before	After	%LOI
1	43.541	68.454	68.099	1.42%
2	50.491	75.099	74.725	1.52%
3	50.470	75.178	74.828	1.42%
%LOI	Std Dev	0.06%	Avg	1.45%

LOI-Z				
	Crucible	Before	After	%LOI
1	47.348	72.768	72.393	1.48%
2	49.046	74.163	73.816	1.38%
3	19.300	44.444	44.083	1.44%
%LOI	Std Dev	0.05%	Avg	1.43%

Y-Axis				
Sample	Mass	Tensile	Scratch	Perm
1	88.3	171.4	52	400
2	88.6	194.2	59	400
3	88.8	186.2	57	420
4	87.9	200.6	57	440
5	88.9	190.6	56	400
6	87.8	187.6	55	420
7	88.4	194.6	53	390
8	88.3	171.4	53	400
9	88.5	192.4	52	400
10	88.5	181.8	55.0	400.0
Avg	88.4	187.08	54.9	407
Std Dev	0.350	9.726	2.378	14.944

X-Density Block				
Sample	Mass	X-Axis	Y-Axis	Z-Axis
1	18.544	1.543	1.037	0.54
2	19.083	1.536	1.032	0.552
3	17.963	1.541	1.032	0.524
4	17.961	1.539	1.038	0.525
Avg	18.388	1.540	1.035	0.535

LOI-Y				
	Crucible	Before	After	%LOI
1	48.081	73.337	72.968	1.46%
2	46.010	71.004	70.645	1.44%
3	51.867	76.922	76.555	1.46%
%LOI	Std Dev	0.02%	Avg	1.45%

Y-Density Block				
Sample	Mass	X-Axis	Y-Axis	Z-Axis
1	18.374	1.034	1.532	0.539
2	17.771	1.03	1.541	0.521
3	17.763	1.035	1.532	0.527
4	18.904	1.032	1.536	0.555
Avg	18.203	1.033	1.535	0.536

Z-Density Block				
Sample	Mass	X-Axis	Y-Axis	Z-Axis
1	18.125	0.531	1.04	1.52
2	17.774	0.529	1.035	1.523
3	17.965	0.533	1.033	1.524
4	18.189	0.535	1.04	1.524
Avg	18.013	0.532	1.037	1.523

Table A3 Collected data set for test series 3A and machine parameters.

Print Order		Test	Sand
DOE Trial #	3	3A	530

X-Res	Z-Res
0.12	0.28

X-Axis				
Sample	Mass	Tensile	Scratch	Perm
1	85.1	160.8	50.0	480.0
2	86.0	125.6	53.0	460.0
3	86.3	129.2	51.0	440.0
4	86.9	158.0	51.0	420.0
5	85.9	141.2	49.0	480.0
6	86.1	157.4	55.0	440.0
7	86.7	164.0	54.0	440.0
8	86.3	160.6	54.0	440.0
9	85.8	144.6	51.0	460.0
10	85.8	156.8	50.0	460.0
Avg	86.09	149.82	51.8	452
Std Dev	0.507	13.841	2.044	19.322

Z-Axis				
Sample	Mass	Tensile	Scratch	Perm
1	85.9	122.2	45	500
2	86.6	123.6	42	440
3	87.6	145.6	44	440
4	87.2	140.6	45	440
5	87.3	128.8	44	440
6	86.1	100	37	500
7	86.1	104.2	39	500
8	86.8	111	40	440
9	87.7	112.4	40	420
10	85.5	109.6	46	480
Avg	86.68	119.8	42.2	460
Std Dev	0.763	15.170	3.048	31.269

LOI-X				
	Crucible	Before	After	%LOI
1	19.927	44.319	43.977	1.40%
2	33.709	58.882	58.523	1.43%
3	34.479	59.551	59.200	1.40%
%LOI	Std Dev	0.01%	Avg	1.41%

LOI-Z				
	Crucible	Before	After	%LOI
1	31.496	56.805	56.489	1.25%
2	36.523	61.632	61.294	1.35%
3	49.047	74.326	73.983	1.36%
%LOI	Std Dev	0.06%	Avg	1.32%

Y-Axis				
Sample	Mass	Tensile	Scratch	Perm
1	85.7	153.6	43	440
2	85.6	150.8	49	440
3	87.2	177.2	47	400
4	86.2	156.2	43	420
5	86.5	166.4	46	440
6	86.4	139.6	38	440
7	86.6	165.6	47	440
8	86.9	140.6	46	420
9	86.8	164	49	420
10	86.7	174.6	51.0	400.0
Avg	86.46	158.86	45.9	426
Std Dev	0.508	12.982	3.755	16.465

X-Density Block				
Sample	Mass	X-Axis	Y-Axis	Z-Axis
1	18.133	1.53	1.032	0.536
2	17.604	1.53	1.025	0.526
3	18.056	1.529	1.029	0.534
4	17.695	1.531	1.032	0.524
Avg	17.872	1.530	1.030	0.530

LOI-Y				
	Crucible	Before	After	%LOI
1	34.729	59.136	58.801	1.37%
2	30.408	55.364	55.051	1.25%
3	32.797	57.914	57.579	1.33%
%LOI	Std Dev	0.06%	Avg	1.32%

Y-Density Block				
Sample	Mass	X-Axis	Y-Axis	Z-Axis
1	17.952	1.036	1.533	0.538
2	17.597	1.037	1.532	0.528
3	17.439	1.031	1.532	0.538
4	17.512	1.035	1.536	0.528
Avg	17.625	1.035	1.533	0.533

Z-Density Block				
Sample	Mass	X-Axis	Y-Axis	Z-Axis
1	17.829	0.537	1.034	1.533
2	17.556	0.53	1.028	1.529
3	17.715	0.537	1.03	1.534
4	18.028	0.53	1.034	1.535
Avg	17.782	0.534	1.032	1.533

Table A4 Collected data set for test series 4A and machine parameters.

	Print Order	Test	Sand
DOE Trial #	4	4A	530

X-Res	Z-Res
0.12	0.39

X-Axis				
Sample	Mass	Tensile	Scratch	Perm
1	85.7	103.8	41.0	440.0
2	85.9	120.4	31.0	440.0
3	85.7	125.2	36.0	460.0
4	85.6	120.2	34.0	440.0
5	86.0	114.4	41.0	440.0
6	86.1	115.0	42.0	420.0
7	86.0	120.8	43.0	440.0
8	85.8	124.4	43.0	440.0
9	86.3	115.8	35.0	420.0
10	86.4	119.0	30.0	440.0
Avg	85.95	117.9	37.6	438
Std Dev	0.264	6.152	4.993	11.353

LOI-X				
	Crucible	Before	After	%LOI
1	50.493	74.713	74.470	1.00%
2	43.529	68.416	68.173	0.98%
3	50.596	75.327	75.074	1.02%
%LOI	Std Dev	0.02%	Avg	1.00%

Y-Axis				
Sample	Mass	Tensile	Scratch	Perm
1	85.7	100.8	39	440
2	86.1	107.8	33	400
3	86.4	112.8	39	420
4	86.5	117.2	41	420
5	85.4	108	39	460
6	86.8	128.8	40	440
7	86.2	109.2	34	440
8	86	111	42	420
9	85.4	115	38	440
10	85.7	112.8	35.0	440.0
Avg	86.02	112.34	38	432
Std Dev	0.471	7.351	3.018	16.865

LOI-Y				
	Crucible	Before	After	%LOI
1	48.085	73.467	73.209	1.02%
2	46.012	71.103	70.847	1.02%
3	51.872	76.584	76.347	0.96%
%LOI	Std Dev	0.03%	Avg	1.00%

Z-Axis				
Sample	Mass	Tensile	Scratch	Perm
1	85.4	78	22	500
2	84.9	86.4	34	480
3	86.1	100	31	480
4	86.1	107.6	38	440
5	86.2	112	37	440
6	85.2	91	34	460
7	85	71.6	29	440
8	85.9	69	24	440
9	85.2	82.2	31	420
10	86.4	108.2	33	440
Avg	85.64	90.6	31.3	454
Std Dev	0.556	15.705	5.165	25.033

LOI-Z				
	Crucible	Before	After	%LOI
1	47.351	72.686	72.434	0.99%
2	49.047	74.730	74.488	0.94%
3	19.932	44.978	44.752	0.90%
%LOI	Std Dev	0.05%	Avg	0.95%

X-Density Block				
Sample	Mass	X-Axis	Y-Axis	Z-Axis
1	17.11	1.525	1.029	0.518
2	17.234	1.525	1.025	0.515
3	17.911	1.524	1.028	0.534
4	18.407	1.524	1.028	0.548
Avg	17.666	1.525	1.028	0.529

Y-Density Block				
Sample	Mass	X-Axis	Y-Axis	Z-Axis
1	17.176	1.031	1.526	0.517
2	17.317	1.035	1.532	0.518
3	17.85	1.039	1.531	0.533
4	18.33	1.03	1.531	0.552
Avg	17.668	1.034	1.530	0.530

Z-Density Block				
Sample	Mass	X-Axis	Y-Axis	Z-Axis
1	17.5	0.528	1.031	1.513
2	17.459	0.53	1.027	1.519
3	17.372	0.526	1.029	1.518
4	17.67	0.531	1.036	1.517
Avg	17.500	0.529	1.031	1.517

Table A5 Collected data set for test series 5A and machine parameters.

	Print Order	Test	Sand
DOE Trial #	5	5A	510

X-Res	Z-Res
0.08	0.28

X-Axis

Sample	Mass	Tensile	Scratch	Perm
1	85.2	240.8	65.0	250.0
2	84.4	242.0	64.0	250.0
3	84.0	230.8	64.0	260.0
4	84.9	235.4	61.0	250.0
5	84.7	224.6	62.0	250.0
6	84.7	215.8	61.0	250.0
7	84.8	214.2	62.0	250.0
8	85.2	217.2	60.0	260.0
9	84.7	263.0	60.0	250.0
10	84.5	225.0	64.0	250.0
Avg	84.71	230.88	62.3	252
Std Dev	0.360	15.059	1.829	4.216

LOI-X

	Crucible	Before	After	%LOI
1	50.491	74.889	74.393	2.03%
2	43.525	68.335	67.869	1.88%
3	50.480	75.409	74.933	1.91%
%LOI	Std Dev	0.08%	Avg	1.94%

Y-Axis

Sample	Mass	Tensile	Scratch	Perm
1	85.2	221.3	61	250
2	85.3	245.8	61	240
3	84.9	253.2	63	250
4	84.1	228	61	250
5	85.4	220	63	240
6	85.2	272.6	61	250
7	83.8	229	64	250
8	84.9	233	63	240
9	84.4	228.8	61	240
10	83.7	214.8	62.0	250.0
Avg	84.69	234.65	62	246
Std Dev	0.640	17.665	1.155	5.164

LOI-Y

	Crucible	Before	After	%LOI
1	48.082	73.552	73.055	1.95%
2	46.014	69.779	69.307	1.99%
3	51.871	76.074	75.594	1.98%
%LOI	Std Dev	0.02%	Avg	1.97%

Z-Axis

Sample	Mass	Tensile	Scratch	Perm
1	85.4	242.4	65	240
2	83.4	198.4	59	260
3	84.7	216	62	260
4	85.6	240.8	64	250
5	85.7	224.2	61	250
6	84.7	195.4	58	270
7	84.7	221.8	60	250
8	85.2	214.8	59	270
9	86.6	240.2	63	250
10	84.5	234	60	250
Avg	85.05	222.8	61.1	255
Std Dev	0.861	16.983	2.331	9.718

LOI-Z

	Crucible	Before	After	%LOI
1	47.348	72.164	71.687	1.92%
2	49.049	74.153	73.648	2.01%
3	19.928	40.300	39.912	1.90%
%LOI	Std Dev	0.06%	Avg	1.95%

X-Density Block

Sample	Mass	X-Axis	Y-Axis	Z-Axis
1	17.47	1.53	1.026	0.523
2	17.831	1.528	1.027	0.535
3	17.863	1.532	1.026	0.538
4	17.354	1.531	1.027	0.527
Avg	17.630	1.530	1.027	0.531

Y-Density Block

Sample	Mass	X-Axis	Y-Axis	Z-Axis
1	17.234	1.025	1.527	0.529
2	17.611	1.026	1.527	0.535
3	17.201	1.027	1.53	0.525
4	17.624	1.025	1.527	0.537
Avg	17.418	1.026	1.528	0.532

Z-Density Block

Sample	Mass	X-Axis	Y-Axis	Z-Axis
1	17.473	0.531	1.033	1.525
2	17.442	0.529	1.03	1.529
3	17.22	0.526	1.026	1.532
4	17.65	0.534	1.037	1.531
Avg	17.446	0.530	1.032	1.529

Table A6 Collected data set for test series 6A and machine parameters.

	Print Order		Test	Sand
DOE Trial #	6		6A	510

X-Res	Z-Res
0.08	0.39

X-Axis				
Sample	Mass	Tensile	Scratch	Perm
1	82.4	167.0	53.0	280.0
2	82.5	163.8	52.0	280.0
3	82.7	154.8	56.0	260.0
4	83.2	165.4	56.0	270.0
5	82.4	159.2	56.0	280.0
6	82.7	166.0	56.0	280.0
7	82.4	148.8	54.0	280.0
8	82.7	170.8	54.0	280.0
9	83.0	160.6	58.0	270.0
10	82.4	157.0	54.0	290.0
Avg	82.64	161.34	54.9	277
Std Dev	0.280	6.581	1.792	8.233

LOI-X				
	Crucible	Before	After	%LOI
1	50.503	75.705	75.302	1.60%
2	43.530	68.510	68.130	1.52%
3	50.502	75.280	74.899	1.54%
%LOI	Std Dev	0.04%	Avg	1.55%

Y-Axis				
Sample	Mass	Tensile	Scratch	Perm
1	82.8	178.4	54	280
2	82.2	167.2	55	280
3	82.9	164.4	52	270
4	82.5	165.6	54	280
5	82.8	176.6	52	280
6	81.7	143.8	57	290
7	82.6	155.6	54	290
8	82.1	169.2	56	280
9	83	166	54	280
10	82.2	164.4	56.0	280.0
Avg	82.48	165.12	54.4	281
Std Dev	0.418	9.868	1.647	5.676

LOI-Y				
	Crucible	Before	After	%LOI
1	48.092	72.936	72.551	1.55%
2	46.047	70.861	70.478	1.54%
3	51.875	76.331	75.955	1.54%
%LOI	Std Dev	0.01%	Avg	1.54%

Z-Axis				
Sample	Mass	Tensile	Scratch	Perm
1	82.6	147.4	53	280
2	83	158.4	53	290
3	83.4	153	52	280
4	83	158	57	280
5	81.2	132.6	52	280
6	82.4	156.8	56	280
7	82.1	155.2	57	290
8	83.3	144.4	53	280
9	82.3	150	54	290
10	83.6	139	54	290
Avg	82.69	149.48	54.1	284
Std Dev	0.723	8.667	1.912	5.164

LOI-Z				
	Crucible	Before	After	%LOI
1	47.358	72.314	71.928	1.55%
2	49.051	73.995	73.611	1.54%
3	19.937	44.553	44.165	1.58%
%LOI	Std Dev	0.02%	Avg	1.55%

X-Density Block				
Sample	Mass	X-Axis	Y-Axis	Z-Axis
1	17.099	1.524	1.022	0.53
2	16.677	1.527	1.024	0.516
3	16.547	1.53	1.023	0.51
4	17.709	1.527	1.026	0.547
Avg	17.008	1.527	1.024	0.526

Y-Density Block				
Sample	Mass	X-Axis	Y-Axis	Z-Axis
1	17.136	1.027	1.525	0.526
2	17.63	1.026	1.526	0.547
3	16.624	1.027	1.523	0.516
4	16.564	1.023	1.53	0.516
Avg	16.989	1.026	1.526	0.526

Z-Density Block				
Sample	Mass	X-Axis	Y-Axis	Z-Axis
1	16.873	0.528	1.031	1.51
2	16.585	0.523	1.021	1.516
3	16.866	0.526	1.032	1.512
4	16.816	0.534	1.028	1.516
Avg	16.785	0.528	1.028	1.514

Table A7 Collected data set for test series 7A and machine parameters.

Print Order		Test	Sand
DOE Trial #	7	7A	510

X-Res	Z-Res
0.12	0.28

X-Axis				
Sample	Mass	Tensile	Scratch	Perm
1	84.3	187.8	54.0	250.0
2	83.4	191.0	56.0	270.0
3	84.4	166.4	57.0	250.0
4	84.8	176.4	56.0	260.0
5	84.9	172.6	58.0	250.0
6	84.4	193.0	58.0	260.0
7	85.0	171.8	57.0	250.0
8	84.3	201.6	59.0	260.0
9	84.2	173.8	55.0	250.0
10	84.2	165.2	54.0	240.0
Avg	84.39	179.96	56.4	254
Std Dev	0.456	12.449	1.713	8.433

Z-Axis				
Sample	Mass	Tensile	Scratch	Perm
1	84.8	166.8	56	250
2	82.6	136.6	52	270
3	83.9	160.8	55	270
4	83.9	151.6	51	260
5	84.8	166	50	260
6	84	134.8	48	290
7	83.8	153	54	280
8	84.9	152.8	52	260
9	84.2	173.2	54	250
10	85.3	147.4	52	250
Avg	84.22	154.3	52.4	264
Std Dev	0.771	12.671	2.413	13.499

LOI-X				
	Crucible	Before	After	%LOI
1	50.495	75.268	74.931	1.36%
2	43.529	67.605	67.300	1.27%
3	50.499	75.829	75.496	1.31%
%LOI	Std Dev	0.05%	Avg	1.31%

LOI-Z				
	Crucible	Before	After	%LOI
1	47.360	72.597	72.264	1.32%
2	49.050	74.374	74.061	1.24%
3	19.931	44.764	44.448	1.27%
%LOI	Std Dev	0.04%	Avg	1.28%

Y-Axis				
Sample	Mass	Tensile	Scratch	Perm
1	83.8	167.2	55	250
2	84.6	178.8	57	240
3	82.2	200.4	55	260
4	84.2	190.6	56	250
5	83.6	172.4	57	260
6	84.1	157.8	53	250
7	84.1	186.6	55	250
8	84.3	179	55	260
9	84.1	177.4	55	260
10	84.3	185.8	55.0	260.0
Avg	83.93	179.6	55.3	254
Std Dev	0.667	12.146	1.160	6.992

X-Density Block				
Sample	Mass	X-Axis	Y-Axis	Z-Axis
1	17.263	1.524	1.028	0.52
2	17.542	1.524	1.022	0.534
3	17.683	1.521	1.027	0.538
4	17.235	1.528	1.028	0.523
Avg	17.431	1.524	1.026	0.529

LOI-Y				
	Crucible	Before	After	%LOI
1	48.087	72.768	72.469	1.21%
2	46.024	71.214	70.887	1.30%
3	51.876	76.564	76.236	1.33%
%LOI	Std Dev	0.06%	Avg	1.28%

Y-Density Block				
Sample	Mass	X-Axis	Y-Axis	Z-Axis
1	17.165	1.029	1.526	0.525
2	17.173	1.028	1.528	0.524
3	17.526	1.033	1.524	0.539
4	17.446	1.031	1.524	0.529
Avg	17.328	1.030	1.526	0.529

Z-Density Block				
Sample	Mass	X-Axis	Y-Axis	Z-Axis
1	17.225	0.529	1.026	1.537
2	17.6	0.532	1.033	1.534
3	17.483	0.532	1.033	1.532
4	17.371	0.529	1.034	1.534
Avg	17.420	0.531	1.032	1.534

Table A8 Collected data set for test series 8A and machine parameters.

	Print Order	Test	Sand
DOE Trial #	8	8A	510

X-Res	Z-Res
0.12	0.39

X-Axis				
Sample	Mass	Tensile	Scratch	Perm
1	83.1	115.0	46.0	240.0
2	82.8	111.4	47.0	240.0
3	83.9	107.2	35.0	230.0
4	82.3	118.4	39.0	260.0
5	82.6	120.6	51.0	240.0
6	82.6	104.0	39.0	260.0
7	82.7	122.6	41.0	250.0
8	83.4	118.4	39.0	250.0
9	83.6	119.0	43.0	230.0
10	83.6	109.2	34.0	230.0
Avg	83.06	114.58	41.4	243
Std Dev	0.538	6.280	5.379	11.595

Z-Axis				
Sample	Mass	Tensile	Scratch	Perm
1	83.8	90.8	38	230
2	83.5	57.8	27	240
3	82.5	47.6	26	250
4	82.4	69	31	250
5	83.5	72.6	39	250
6	82.7	65.8	36	250
7	83.1	65.8	37	240
8	82.5	69.4	39	250
9	83.3	77.2	42	250
10	83.9	90	41	230
Avg	83.12	70.6	35.6	244
Std Dev	0.563	13.228	5.661	8.433

LOI-X				
	Crucible	Before	After	%LOI
1	50.476	75.515	75.253	1.05%
2	50.497	75.408	75.165	0.98%
3	43.530	68.478	68.220	1.03%
%LOI	Std Dev	0.04%	Avg	1.02%

LOI-Z				
	Crucible	Before	After	%LOI
1	47.355	72.505	72.249	1.02%
2	49.053	73.761	73.522	0.97%
3	19.937	44.447	44.218	0.93%
%LOI	Std Dev	0.04%	Avg	0.97%

Y-Axis				
Sample	Mass	Tensile	Scratch	Perm
1	83.7	110	42	220
2	83.3	117	47	230
3	82.6	107.2	45	240
4	83.4	111.8	39	250
5	83.4	97.4	41	230
6	82.8	88.6	36	230
7	83.4	110.2	44	230
8	83.3	107.4	41	240
9	83	105.4	44	230
10	82.5	107.4	42.0	240.0
Avg	83.14	106.24	42.1	234
Std Dev	0.395	7.959	3.143	8.433

X-Density Block				
Sample	Mass	X-Axis	Y-Axis	Z-Axis
1	16.556	1.514	1.014	0.503
2	17.045	1.52	1.019	0.522
3	16.249	1.515	1.013	0.506
4	17.624	1.521	1.017	0.538
Avg	16.869	1.518	1.016	0.517

LOI-Y				
	Crucible	Before	After	%LOI
1	46.018	70.633	70.381	1.02%
2	48.083	73.152	72.913	0.95%
3	51.872	76.212	75.982	0.94%
%LOI	Std Dev	0.04%	Avg	0.97%

Y-Density Block				
Sample	Mass	X-Axis	Y-Axis	Z-Axis
1	17.48	1.021	1.519	0.538
2	16.98	1.021	1.517	0.526
3	16.394	1.027	1.518	0.507
4	16.421	1.017	1.519	0.506
Avg	16.819	1.022	1.518	0.519

Z-Density Block				
Sample	Mass	X-Axis	Y-Axis	Z-Axis
1	16.528	0.518	1.016	1.51
2	16.883	0.522	1.02	1.513
3	16.621	0.519	1.019	1.51
4	16.679	0.519	1.021	1.509
Avg	16.678	0.520	1.019	1.511

Table A9 Collected data set for test series 1B and machine parameters.

	Print Order	Test	Sand
DOE Trial #	9	1B	530

X-Res	Z-Res
0.08	0.28

X-Axis				
Sample	Mass	Tensile	Scratch	Perm
1	89.6	221.2	60.0	420.0
2	87.6	182.2	56.0	500.0
3	88.3	193.6	64.0	480.0
4	88.4	203.4	57.0	500.0
5	89.3	192.8	56.0	460.0
6	88.9	214.8	59.0	480.0
7	89.1	231.6	59.0	460.0
8	89.0	219.8	61.0	440.0
9	88.7	208.2	61.0	440.0
10	88.0	202.8	57.0	460.0
Avg	88.69	207.04	59	464
Std Dev	0.615	15.128	2.582	26.331

Z-Axis				
Sample	Mass	Tensile	Scratch	Perm
1	90.1	198.4	61	440
2	87.6	188.6	57	480
3	88.5	188	56	480
4	90.2	178	59	500
5	89.4	205.4	55	440
6	88.6	166.8	45	500
7	88.6	186.4	56	480
8	90.8	219.8	59	480
9	90	201.6	60	440
10	90.1	212.4	56	480
Avg	89.39	194.54	56.4	472
Std Dev	1.015	16.080	4.477	23.476

LOI-X				
	Crucible	Before	After	%LOI
1	43.526	69.482	68.997	1.87%
2	50.471	76.114	75.637	1.86%
3	50.492	76.075	75.613	1.81%
%LOI	Std Dev	0.03%	Avg	1.84%

LOI-Z				
	Crucible	Before	After	%LOI
1	47.348	72.335	71.925	1.64%
2	49.050	74.147	73.703	1.77%
3	19.933	45.059	44.628	1.72%
%LOI	Std Dev	0.06%	Avg	1.71%

Y-Axis				
Sample	Mass	Tensile	Scratch	Perm
1	89.4	238.2	59	460
2	89.4	231.8	57	440
3	89.3	216.8	59	440
4	88.7	247.8	57	440
5	88.6	216.6	58	440
6	88.6	229.2	55	460
7	89.1	256	57	460
8	89.4	245	54	460
9	87.4	231.4	57	480
10	87.8	212.6	58.0	480.0
Avg	88.77	232.54	57.1	456
Std Dev	0.704	14.464	1.595	15.776

X-Density Block				
Sample	Mass	X-Axis	Y-Axis	Z-Axis
1	18.886	1.548	1.041	0.543
2	18.565	1.547	1.042	0.531
3	18.908	1.55	1.047	0.546
4	18.547	1.55	1.04	0.531
Avg	18.727	1.549	1.043	0.538

LOI-Y				
	Crucible	Before	After	%LOI
1	51.869	76.802	76.355	1.79%
2	46.010	71.060	70.606	1.81%
3	48.084	73.419	72.966	1.79%
%LOI	Std Dev	0.01%	Avg	1.80%

Y-Density Block				
Sample	Mass	X-Axis	Y-Axis	Z-Axis
1	18.558	1.041	1.541	0.55
2	18.655	1.048	1.544	0.546
3	18.067	1.041	1.539	0.534
4	18.179	1.044	1.54	0.536
Avg	18.365	1.044	1.541	0.542

Z-Density Block				
Sample	Mass	X-Axis	Y-Axis	Z-Axis
1	18.398	0.543	1.047	1.538
2	18.155	0.544	1.04	1.549
3	18.659	0.55	1.049	1.535
4	18.596	0.548	1.042	1.533
Avg	18.452	0.546	1.045	1.539

Table A10 Collected data set for test series 2B and machine parameters.

	Print Order	Test	Sand
DOE Trial #	10	2B	530

X-Res	Z-Res
0.08	0.39

X-Axis

Sample	Mass	Tensile	Scratch	Perm
1	89.1	178.2	57.0	420.0
2	88.9	183.8	57.0	460.0
3	89.1	185.5	55.0	440.0
4	88.9	179.2	51.0	440.0
5	89.3	174.8	55.0	400.0
6	88.2	164.6	54.0	420.0
7	88.2	190.0	50.0	420.0
8	88.5	165.8	59.0	460.0
9	88.8	195.2	57.0	460.0
10	89.1	172.4	55.0	440.0
Avg	88.81	178.95	55	436
Std Dev	0.387	9.956	2.789	20.656

LOI-X

	Crucible	Before	After	%LOI
1	43.525	68.947	68.582	1.44%
2	50.473	75.646	75.285	1.43%
3	50.493	75.157	74.810	1.41%
%LOI	Std Dev	0.02%	Avg	1.43%

Y-Axis

Sample	Mass	Tensile	Scratch	Perm
1	88.3	197.8	54	440
2	89.6	189.8	53	400
3	89.3	177.4	56	420
4	89	194.6	52	410
5	88.7	171	54	440
6	88.1	173.6	51	440
7	88.9	185.4	59	420
8	88.9	200.2	53	420
9	89	188	55	400
10	89.2	189.0	53.0	400.0
Avg	88.9	186.68	54	419
Std Dev	0.447	9.948	2.261	16.633

LOI-Y

	Crucible	Before	After	%LOI
1	51.869	76.743	76.383	1.45%
2	46.013	71.320	70.958	1.43%
3	48.084	73.473	73.110	1.43%
%LOI	Std Dev	0.01%	Avg	1.44%

Z-Axis

Sample	Mass	Tensile	Scratch	Perm
1	89.2	160.8	54	420
2	87.5	133.6	47	460
3	88.7	174.8	49	480
4	89.7	146	45	440
5	88.7	138.8	47	440
6	88.4	138.6	45	480
7	88.2	153.4	55	440
8	89.6	135.6	50	420
9	89	148.8	49	440
10	89.7	160.2	51	420
Avg	88.87	149.06	49.2	444
Std Dev	0.718	13.282	3.425	22.706

LOI-Z

	Crucible	Before	After	%LOI
1	47.350	72.421	72.068	1.41%
2	49.051	74.235	73.906	1.31%
3	19.934	44.840	44.498	1.37%
%LOI	Std Dev	0.05%	Avg	1.36%

X-Density Block

Sample	Mass	X-Axis	Y-Axis	Z-Axis
1	19.196	1.535	1.038	0.555
2	18.676	1.54	1.037	0.543
3	18.076	1.542	1.044	0.523
4	17.96	1.539	1.035	0.523
Avg	18.477	1.539	1.039	0.536

Y-Density Block

Sample	Mass	X-Axis	Y-Axis	Z-Axis
1	17.878	1.039	1.54	0.523
2	17.821	1.039	1.551	0.527
3	18.321	1.034	1.535	0.545
4	18.919	1.039	1.532	0.557
Avg	18.235	1.038	1.540	0.538

Z-Density Block

Sample	Mass	X-Axis	Y-Axis	Z-Axis
1	18.116	0.545	1.043	1.519
2	18.083	0.538	1.033	1.525
3	17.909	0.535	1.037	1.523
4	18.375	0.54	1.043	1.523
Avg	18.121	0.540	1.039	1.523

Table A11 Collected data set for test series 3B and machine parameters.

Print Order		Test	Sand
DOE Trial #	11	3B	530

X-Res	Z-Res
0.12	0.28

X-Axis

Sample	Mass	Tensile	Scratch	Perm
1	84.7	130.6	48.0	500.0
2	85.5	134.2	49.0	500.0
3	84.9	119.2	48.0	500.0
4	86.5	151.4	42.0	420.0
5	86.2	154.2	48.0	420.0
6	87.0	157.4	51.0	440.0
7	86.5	149.2	51.0	460.0
8	85.7	132.0	44.0	480.0
9	85.9	136.0	43.0	480.0
10	85.1	115.2	42.0	480.0
Avg	85.8	137.94	46.6	468
Std Dev	0.760	14.630	3.534	31.552

LOI-X

	Crucible	Before	After	%LOI
1	50.491	75.922	75.599	1.27%
2	43.526	68.300	67.987	1.26%
3	50.473	75.178	74.864	1.27%
%LOI	Std Dev	0.00%	Avg	1.27%

Y-Axis

Sample	Mass	Tensile	Scratch	Perm
1	86.3	171.6	49	440
2	86.9	152	51	460
3	86.3	149.6	58	440
4	85.9	152	47	460
5	85.1	136	45	460
6	84.6	148.2	49	480
7	84.9	149.8	49	480
8	85.6	131	37	480
9	85.9	142.6	45	480
10	86.7	144.4	46.0	440.0
Avg	85.82	147.72	47.6	462
Std Dev	0.769	10.899	5.317	17.512

LOI-Y

	Crucible	Before	After	%LOI
1	51.868	76.641	76.340	1.22%
2	46.011	70.902	70.596	1.23%
3	48.083	73.539	73.233	1.20%
%LOI	Std Dev	0.01%	Avg	1.22%

Z-Axis

Sample	Mass	Tensile	Scratch	Perm
1	87.2	142.4	50	440
2	84.7	102.8	38	500
3	85.2	118.4	40	500
4	87.4	118.6	43	480
5	86.4	103.8	47	460
6	85.2	80.6	39	400
7	85.5	97.4	39	500
8	87.5	84.8	39	440
9	87.2	97.4	40	480
10	86.9	133.8	46	500
Avg	86.32	108	42.1	470
Std Dev	1.067	20.077	4.175	34.319

LOI-Z

	Crucible	Before	After	%LOI
1	47.349	72.227	71.934	1.18%
2	49.049	71.565	71.305	1.15%
3	19.932	44.280	43.976	1.25%
%LOI	Std Dev	0.05%	Avg	1.19%

X-Density Block

Sample	Mass	X-Axis	Y-Axis	Z-Axis
1	17.532	1.533	1.032	0.523
2	17.973	1.539	1.037	0.539
3	17.975	1.543	1.026	0.536
4	17.562	1.536	1.025	0.526
Avg	17.761	1.538	1.030	0.531

Y-Density Block

Sample	Mass	X-Axis	Y-Axis	Z-Axis
1	17.554	1.037	1.542	0.529
2	17.918	1.043	1.545	0.542
3	17.869	1.035	1.537	0.541
4	17.356	1.037	1.532	0.523
Avg	17.674	1.038	1.539	0.534

Z-Density Block

Sample	Mass	X-Axis	Y-Axis	Z-Axis
1	17.686	0.534	1.038	1.531
2	17.682	0.537	1.038	1.534
3	17.475	0.538	1.031	1.534
4	17.684	0.533	1.034	1.529
Avg	17.632	0.536	1.035	1.532

Table A12 Collected data set for test series 4B and machine parameters.

	Print Order	Test	Sand
DOE Trial #	12	4B	530

X-Res	Z-Res
0.12	0.39

X-Axis

Sample	Mass	Tensile	Scratch	Perm
1	86.0	122.0	43.0	400.0
2	86.6	121.0	45.0	420.0
3	86.0	123.8	40.0	420.0
4	86.1	105.8	33.0	420.0
5	85.8	107.0	29.0	460.0
6	86.2	101.0	37.0	400.0
7	85.9	95.4	36.0	440.0
8	86.1	110.0	35.0	420.0
9	86.2	113.0	39.0	440.0
10	86.1	105.8	40.0	410.0
Avg	86.1	110.48	37.7	423
Std Dev	0.216	9.431	4.739	18.886

LOI-X

	Crucible	Before	After	%LOI
1	34.506	55.557	55.342	1.02%
2	31.595	53.784	53.559	1.01%
3	31.090	51.390	51.185	1.01%
%LOI	Std Dev	0.01%	Avg	1.02%

Y-Axis

Sample	Mass	Tensile	Scratch	Perm
1	86.8	114	35	400
2	86.6	112	40	400
3	86.8	108.2	41	420
4	86.4	111.4	42	420
5	85.7	86.6	32	420
6	85.8	91.8	32	420
7	86.2	102.4	38	440
8	86	116.8	33	460
9	85.9	114.4	38	420
10	86.7	95.8	37.0	440.0
Avg	86.29	105.34	36.8	424
Std Dev	0.425	10.603	3.676	18.379

LOI-Y

	Crucible	Before	After	%LOI
1	49.049	69.227	69.046	0.90%
2	36.517	56.439	56.241	0.99%
3	19.930	43.178	42.971	0.89%
%LOI	Std Dev	0.06%	Avg	0.93%

Z-Axis

Sample	Mass	Tensile	Scratch	Perm
1	86.4	80.6	39	420
2	86.3	89.8	38	420
3	85.1	60.4	33	440
4	86	81.8	30	440
5	86.9	89.8	33	420
6	85.9	54	28	440
7	83.2	74.6	25	440
8	86.3	56.2	25	420
9	85.8	55	23	440
10	85.6	68.2	28	420
Avg	85.75	71.04	30.2	430
Std Dev	1.021	14.193	5.473	10.541

LOI-Z

	Crucible	Before	After	%LOI
1	30.417	52.231	52.019	0.97%
2	34.733	55.786	55.579	0.98%
3	33.711	54.612	54.407	0.98%
%LOI	Std Dev	0.01%	Avg	0.98%

X-Density Block

Sample	Mass	X-Axis	Y-Axis	Z-Axis
1	17.673	1.525	1.027	0.531
2	17.159	1.534	1.023	0.516
3	18.185	1.528	1.024	0.546
4	17.142	1.529	1.026	0.516
Avg	17.540	1.529	1.025	0.527

Y-Density Block

Sample	Mass	X-Axis	Y-Axis	Z-Axis
1	18.419	1.535	1.037	0.547
2	17.825	1.534	1.029	0.532
3	17.186	1.534	1.032	0.513
4	17.235	1.529	1.031	0.518
Avg	17.666	1.533	1.032	0.528

Z-Density Block

Sample	Mass	X-Axis	Y-Axis	Z-Axis
1	17.409	0.528	1.026	1.519
2	17.474	0.532	1.03	1.516
3	17.435	0.531	1.032	1.52
4	17.538	0.532	1.03	1.513
Avg	17.464	0.531	1.030	1.517

Table A13 Collected data set for test series 5B and machine parameters.

	Print Order		Test	Sand
DOE Trial #	13		5B	510

X-Res	Z-Res
0.08	0.28

X-Axis				
Sample	Mass	Tensile	Scratch	Perm
1	85.8	252.6	65.0	240.0
2	85.4	254.6	64.0	240.0
3	85.6	248.0	60.0	240.0
4	85.9	247.8	59.0	240.0
5	85.4	220.2	63.0	240.0
6	84.5	231.4	62.0	260.0
7	85.2	209.0	61.0	250.0
8	85.7	218.8	60.0	260.0
9	85.9	233.6	63.0	250.0
10	86.2	251.2	59.0	250.0
Avg	85.56	236.72	61.6	247
Std Dev	0.474	16.438	2.119	8.233

LOI-X				
	Crucible	Before	After	%LOI
1	34.507	56.489	56.055	1.97%
2	31.596	55.666	55.187	1.99%
3	31.091	52.879	52.438	2.02%
%LOI	Std Dev	0.03%	Avg	2.00%

Y-Axis				
Sample	Mass	Tensile	Scratch	Perm
1	84.9	226.4	62	250
2	86	227.4	61	240
3	85.8	233.2	62	230
4	85.9	247.8	60	240
5	85.2	222.2	60	240
6	85.3	236.4	62	250
7	85.7	250.2	62	240
8	85.3	227.4	60	240
9	85.7	254	61	240
10	85.0	239.0	62.0	250.0
Avg	85.48	236.4	61.2	242
Std Dev	0.388	11.110	0.919	6.325

LOI-Y				
	Crucible	Before	After	%LOI
1	49.049	75.169	74.660	1.95%
2	36.519	59.393	58.923	2.05%
3	33.264	53.800	53.410	1.90%
%LOI	Std Dev	0.08%	Avg	1.97%

Z-Axis				
Sample	Mass	Tensile	Scratch	Perm
1	84	200.4	60	250
2	85.7	214.4	61	250
3	86.1	250.2	63	250
4	85.4	218	60	250
5	86.5	247.8	63	240
6	85	203.4	64	260
7	86.4	184.6	63	260
8	86.8	198	63	250
9	86.4	241.8	63	250
10	86.9	249.4	61	240
Avg	85.92	220.8	62.1	250
Std Dev	0.908	24.609	1.449	6.667

LOI-Z				
	Crucible	Before	After	%LOI
1	33.708	56.034	55.601	1.94%
2	30.419	53.878	53.425	1.93%
3	34.736	59.761	59.289	1.89%
%LOI	Std Dev	0.03%	Avg	1.92%

X-Density Block				
Sample	Mass	X-Axis	Y-Axis	Z-Axis
1	18.05	1.534	1.033	0.537
2	17.586	1.535	1.026	0.525
3	17.731	1.535	1.027	0.523
4	17.918	1.534	1.029	0.532
Avg	17.821	1.535	1.029	0.529

Y-Density Block				
Sample	Mass	X-Axis	Y-Axis	Z-Axis
1	17.698	1.03	1.535	0.534
2	17.337	1.026	1.53	0.525
3	17.66	1.034	1.528	0.536
4	17.204	1.029	1.527	0.522
Avg	17.475	1.030	1.530	0.529

Z-Density Block				
Sample	Mass	X-Axis	Y-Axis	Z-Axis
1	17.852	0.529	1.036	1.552
2	17.603	0.53	1.032	1.531
3	17.629	0.529	1.031	1.543
4	17.345	0.524	1.027	1.535
Avg	17.607	0.528	1.032	1.540

Table A14 Collected data set for test series 6B and machine parameters.

	Print Order	Test	Sand
DOE Trial #	14	6B	510

X-Res	Z-Res
0.08	0.39

X-Axis

Sample	Mass	Tensile	Scratch	Perm
1	82.1	165.4	56.0	290.0
2	83.0	157.4	55.0	290.0
3	82.4	146.4	53.0	290.0
4	82.5	163.4	53.0	300.0
5	82.3	176.0	54.0	300.0
6	82.3	160.0	54.0	300.0
7	83.4	171.4	54.0	290.0
8	82.2	158.0	53.0	290.0
9	82.7	174.2	56.0	290.0
10	82.4	158.8	53.0	300.0
Avg	82.53	163.1	54.1	294
Std Dev	0.400	9.002	1.197	5.164

LOI-X

	Crucible	Before	After	%LOI
1	33.709	56.060	55.711	1.56%
2	30.419	54.414	54.040	1.56%
3	34.735	56.211	55.915	1.38%
%LOI	Std Dev	0.10%	Avg	1.50%

Y-Axis

Sample	Mass	Tensile	Scratch	Perm
1	81.8	159.2	55	290
2	83.4	175.2	58	280
3	82.4	151	50	290
4	82.3	155.4	54	300
5	81.1	148.4	53	300
6	82.6	178	53	290
7	82.7	180.6	56	280
8	82.7	176	56	290
9	83.2	183.8	55	290
10	81.8	175.0	54.0	290.0
Avg	82.4	168.26	54.4	290
Std Dev	0.690	13.258	2.171	6.667

LOI-Y

	Crucible	Before	After	%LOI
1	34.509	56.831	56.502	1.47%
2	31.598	53.718	53.394	1.46%
3	31.093	51.436	51.125	1.53%
%LOI	Std Dev	0.03%	Avg	1.49%

Z-Axis

Sample	Mass	Tensile	Scratch	Perm
1	82.8	147.8	54	280
2	81.8	142.8	53	300
3	82.8	154.8	55	300
4	82.2	143.8	52	300
5	80.8	117	50	280
6	82.4	132.6	55	300
7	82.4	142.6	50	300
8	82.6	159.2	49	280
9	83.5	154.6	54	280
10	83.3	118.6	52	300
Avg	82.46	141.38	52.4	292
Std Dev	0.768	14.581	2.171	10.328

LOI-Z

	Crucible	Before	After	%LOI
1	49.050	76.535	76.133	1.46%
2	36.521	57.413	57.082	1.58%
3	33.262	55.463	55.130	1.50%
%LOI	Std Dev	0.06%	Avg	1.52%

X-Density Block

Sample	Mass	X-Axis	Y-Axis	Z-Axis
1	17.243	1.532	1.027	0.529
2	16.41	1.534	1.029	0.516
3	17.731	1.535	1.025	0.546
4	16.666	1.53	1.032	0.513
Avg	17.013	1.533	1.028	0.526

Y-Density Block

Sample	Mass	X-Axis	Y-Axis	Z-Axis
1	17.48	1.025	1.525	0.543
2	17.075	1.023	1.528	0.531
3	16.561	1.024	1.532	0.516
4	16.522	1.027	1.535	0.517
Avg	16.910	1.025	1.530	0.527

Z-Density Block

Sample	Mass	X-Axis	Y-Axis	Z-Axis
1	16.94	0.526	1.036	1.518
2	16.812	0.526	1.034	1.511
3	16.814	0.526	1.03	1.521
4	16.588	0.527	1.026	1.523
Avg	16.789	0.526	1.032	1.518

Table A15 Collected data set for test series 7B and machine parameters.

	Print Order	Test	Sand
DOE Trial #	15	7B	510

X-Res	Z-Res
0.12	0.28

X-Axis

Sample	Mass	Tensile	Scratch	Perm
1	84.4	183.6	58.0	240.0
2	84.5	196.6	59.0	240.0
3	84.5	166.2	56.0	230.0
4	84.1	162.2	58.0	240.0
5	84.3	176.2	57.0	250.0
6	84.9	164.4	55.0	250.0
7	83.2	165.0	52.0	260.0
8	84.0	189.4	54.0	250.0
9	83.5	173.2	55.0	260.0
10	84.3	177.2	59.0	250.0
Avg	84.17	175.4	56.3	247
Std Dev	0.501	11.592	2.312	9.487

LOI-X

	Crucible	Before	After	%LOI
1	33.712	55.246	54.981	1.23%
2	30.420	54.157	53.837	1.35%
3	34.736	57.552	57.243	1.35%
%LOI	Std Dev	0.07%	Avg	1.31%

Y-Axis

Sample	Mass	Tensile	Scratch	Perm
1	83.3	186.8	58	250
2	83.3	165.8	56	240
3	83.3	161	56	240
4	84.1	179	57	240
5	84.3	163.8	57	230
6	84.7	161.8	54	240
7	84.7	172.6	57	250
8	84.7	182.2	56	240
9	84.3	191.2	56	240
10	84.7	196.6	58.0	250.0
Avg	84.14	176.08	56.5	242
Std Dev	0.617	12.955	1.179	6.325

LOI-Y

	Crucible	Before	After	%LOI
1	31.093	51.898	51.615	1.36%
2	31.603	52.117	51.836	1.37%
3	34.511	54.546	54.270	1.38%
%LOI	Std Dev	0.01%	Avg	1.37%

Z-Axis

Sample	Mass	Tensile	Scratch	Perm
1	85.2	165.6	56	250
2	84.2	138.6	54	260
3	83.3	120.6	57	260
4	85.8	167.4	48	250
5	84.2	141.8	54	240
6	84.2	110	46	270
7	84.8	139.6	49	270
8	85.8	128.2	48	240
9	85.6	110.2	47	240
10	85.6	151.4	53	240
Avg	84.87	137.34	51.2	252
Std Dev	0.864	20.479	4.022	12.293

LOI-Z

	Crucible	Before	After	%LOI
1	36.522	57.588	57.326	1.24%
2	33.264	55.894	55.598	1.31%
3	49.052	73.665	73.364	1.22%
%LOI	Std Dev	0.04%	Avg	1.26%

X-Density Block

Sample	Mass	X-Axis	Y-Axis	Z-Axis
1	17.163	1.518	1.021	0.517
2	17.489	1.521	1.019	0.527
3	17.597	1.525	1.021	0.528
4	16.984	1.524	1.021	0.513
Avg	17.308	1.522	1.021	0.521

Y-Density Block

Sample	Mass	X-Axis	Y-Axis	Z-Axis
1	17.103	1.029	1.52	0.516
2	17.487	1.024	1.526	0.531
3	17.352	1.024	1.524	0.527
4	17.001	1.033	1.53	0.516
Avg	17.236	1.028	1.525	0.523

Z-Density Block

Sample	Mass	X-Axis	Y-Axis	Z-Axis
1	17.165	0.524	1.02	1.522
2	17.236	0.527	1.026	1.525
3	17.048	0.527	1.023	1.522
4	17.26	0.527	1.032	1.521
Avg	17.177	0.526	1.025	1.523

Table A16 Collected data set for test series 8B and machine parameters.

	Print Order	Test	Sand
DOE Trial #	16	8B	510

X-Res	Z-Res
0.12	0.39

X-Axis				
Sample	Mass	Tensile	Scratch	Perm
1	81.5	75.8	38.0	270.0
2	81.0	101.2	37.0	270.0
3	81.3	84.8	33.0	270.0
4	81.3	88.6	28.0	260.0
5	81.9	111.2	46.0	260.0
6	80.9	87.8	31.0	260.0
7	81.2	90.2	40.0	270.0
8	81.7	102.8	40.0	260.0
9	82.2	109.2	44.0	260.0
10	82.5	79.4	39.0	260.0
Avg	81.55	93.1	37.6	264
Std Dev	0.521	12.289	5.602	5.164

Z-Axis				
Sample	Mass	Tensile	Scratch	Perm
1	82.4	58.8	37	280
2	80.4	42	27	300
3	81.7	50.8	31	290
4	80.8	47.8	28	280
5	82.3	56.4	33	270
6	80.8	37.8	29	270
7	81.6	49	24	290
8	82	37.8	28	280
9	81.3	35.4	20	280
10	82	65.4	30	270
Avg	81.53	48.12	28.7	281
Std Dev	0.685	10.009	4.668	9.944

LOI-X				
	Crucible	Before	After	%LOI
1	33.711	55.079	54.894	0.87%
2	30.419	52.953	52.754	0.88%
3	34.790	56.009	55.810	0.94%
%LOI	Std Dev	0.04%	Avg	0.90%

LOI-Z				
	Crucible	Before	After	%LOI
1	36.523	57.781	57.585	0.92%
2	33.264	53.377	53.199	0.88%
3	49.051	73.210	72.990	0.91%
%LOI	Std Dev	0.02%	Avg	0.91%

Y-Axis				
Sample	Mass	Tensile	Scratch	Perm
1	81.7	95.2	40	260
2	81.6	74.4	32	250
3	82.2	94.8	41	250
4	82.6	92.6	44	250
5	81.1	66	27	260
6	81.4	75.2	36	260
7	81.5	73.47	34	270
8	81.6	89.4	39	270
9	81.5	106	39	250
10	81.6	99.2	39.0	260.0
Avg	81.68	86.627	37.1	258
Std Dev	0.424	13.315	4.954	7.888

X-Density Block				
Sample	Mass	X-Axis	Y-Axis	Z-Axis
1	17.124	1.51	1.015	0.533
2	16.499	1.514	1.018	0.518
3	16.163	1.513	1.019	0.51
4	16.125	1.51	1.015	0.502
Avg	16.478	1.512	1.017	0.516

LOI-Y				
	Crucible	Before	After	%LOI
1	31.094	52.627	52.438	0.88%
2	31.599	53.791	53.582	0.94%
3	34.507	56.144	55.941	0.94%
%LOI	Std Dev	0.04%	Avg	0.92%

Y-Density Block				
Sample	Mass	X-Axis	Y-Axis	Z-Axis
1	16.556	1.021	1.516	0.524
2	16.256	1.024	1.527	0.507
3	17.062	1.021	1.523	0.535
4	16.141	1.026	1.518	0.504
Avg	16.504	1.023	1.521	0.518

Z-Density Block				
Sample	Mass	X-Axis	Y-Axis	Z-Axis
1	16.425	0.519	1.021	1.504
2	16.393	0.519	1.017	1.509
3	16.577	0.52	1.019	1.506
4	16.476	0.519	1.018	1.507
Avg	16.468	0.519	1.019	1.507